AD-A160 357

MULTIPLE SCATTER CROSS SECTIONS FOR ANISOTROPIC KOLMOGOROFF TURBULENCE

Stanford P. Yukon

DTIC
ELECTE
OCT 16 1985
B

DTIC FILE COPY

ROME AIR DEVELOPMENT CENTER
Air Force Systems Command
Griffiss Air Force Base, NY 13441-5700

85 10 16 122

This report has been reviewed by the RADC Public Affairs Office (PA) and is releasable to the National Technical Information Service (NTIS). At NTIS it will be releasable to the general public, including foreign nations.

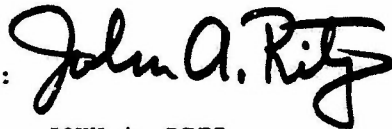RADC-TR-85-22 has been reviewed and is approved for publication.

APPROVED: *[signature]*

TERENCE J. ELKINS
Chief, Propagation Branch
Electromagnetic Sciences Division

APPROVED: *[signature]*

ALLAN C. SCHELL
Chief, Electromagnetic Sciences Division

FOR THE COMMANDER: *[signature]*

JOHN A. RITZ
Acting Chief, Plans Office

If your address has changed or if you wish to be removed from the RADC mailing list, or if the addressee is no longer employed by your organization, please notify RADC (EEPI) Hanscom AFB MA 01731. This will assist us in maintaining a current mailing list.

Do not return copies of this report unless contractual obligations or notices on a specific document requires that it be returned.

REPORT DOCUMENTATION PAGE

1a. REPORT SECURITY CLASSIFICATION	1b. RESTRICTIVE MARKINGS
Unclassified	

2a. SECURITY CLASSIFICATION AUTHORITY	3. DISTRIBUTION/AVAILABILITY OF REPORT
	Approved for public release; distribution unlimited
2b. OECLASSIFICATION/OOWNGRADING SCHEOULE	

4. PERFORMING ORGANIZATION REPORT NUMBER(S)	5. MONITORING ORGANIZATION REPORT NUMBER(S)
RADC-TR-85-22	

6a. NAME OF PERFORMING ORGANIZATION	6b. OFFICE SYMBOL (If applicable)	7a. NAME OF MONITORING ORGANIZATION
Rome Air Development Center	EEPI	Rome Air Development Center (EEPI)

6c. ADORESS (City, State and ZIP Code)	7b. AOORESS (City, State and ZIP Code)
Hanscom AFB Massachusetts 01731	Hanscom AFB Massachusetts 01731

8a. NAME OF FUNOING/SPONSORING ORGANIZATION	8b. OFFICE SYMBOL (If applicable)	9. PROCUREMENT INSTRUMENT IOENTIFICATION NUMBER
Rome Air Development Center	EEPI	

8c. ADORESS (City, State and ZIP Code)	10. SOURCE OF FUNOING NOS.			
Hanscom AFB Massachusetts 01731	PROGRAM ELEMENT NO.	PROJECT NO.	TASK NO.	WORK UNIT NO.

| 11. TITLE (Include Security Classification) Multiple Scatter Cross Sections for (Contd) | 61102F | 4600 | 16 | 08 |

| 12. PERSONAL AUTHOR(S) Yukon, Stanford P. |

13a. TYPE OF REPORT	13b. TIME COVEREO	14. DATE OF REPORT (Yr., Mo., Day)	15. PAGE COUNT
In-house	FROM 9/82 TO 12/83	1985 February	40

16. SUPPLEMENTARY NOTATION

17. COSATI COOES			18. SUBJECT TERMS (Continue on reverse if necessary and identify by block number)
FIELD	GROUP	SUB. GR.	Backscatter; → Random medium; Kolmogoroff
20	03	14	Cross section Propagation; → Green's function;
			Scattering Anisotropic; (Contd)ove.)

19. ABSTRACT (Continue on reverse if necessary and identify by block number)

→ The cross sections for multiple scattering from anisotropic random media are calculated for scattering into forward and backward directions from slabs containing electron density or refractive index irregularities whose symmetry axes are aligned at an arbitrary angle to the slab face. The cross sections are calculated in the CFSB approximation using techniques used in RADC-TR-82-287, and extended here to include arbitrary turbulence spectra and, in particular, three-dimensional Kolmogoroff turbulence. Keywords:

((AD-A127 873))

Cumulative Forward scatter) Single-backscatter)

20. OISTRIBUTION/AVAILABILITY OF ABSTRACT	21. ABSTRACT SECURITY CLASSIFICATION
UNCLASSIFIED/UNLIMITEO ☒ SAME AS RPT. ☐ OTIC USERS ☐	Unclassified

22a. NAME OF RESPONSIBLE INOIVIOUAL	22b. TELEPHONE NUMBER (Include Area Code)	22c. OFFICE SYMBOL
Stanford P. Yukon	(617) 861-2986	EEPI

DD FORM 1473, 83 APR   EOITION OF 1 JAN 73 IS OBSOLETE.

Block 11 (Contd).

Anisotropic Kolmogoroff Turbulence

Block 18 (Contd).

Forward scatter ;
Multiple scatter ;
Ionospheric irregularity ;
Correlation function .

Accession For

NTIS CRA&I	✔
DTIC TAB	☐
Unannounced	☐
Justification	

By
Distribution/

Availability Codes

| Dist | Avail and/or Special |

A-1

DTIC
COPY
INSPECTED

Contents

Illustrations

Multiple Scatter Cross Sections for Anisotropic Kolmogoroff Turbulence

I. INTRODUCTION

In a recent report on backscattering from anisotropic media,[1*] we developed a method for calculating multiple scatter cross sections based on DeWolf's cumulative forward-scatter single-backscatter approximation.[2] The method consisted of obtaining an expression for the scattered wave in terms of the Green's function for a wave propagating in an arbitrary random medium. From this, an expression for the power scattered into an arbitrary direction was obtained. The scattered power obtained from averaging over the random properties of the medium was then expressed as the Fourier transform of a cumulant expansion of the correlation functions for the random medium. To evaluate the Fourier transforms, the cumulant series was further expanded as a functional Taylor series in terms of the projected correlation functions (structure functions) of the medium. Fourier transforms of products of arbitrary powers of correlation functions projected along the incoming and scatter directions were then expressed as convolution

1. Yukon, S.P. (1982) Backscatter From Anisotropic Random Media, RADC-TR-82-287.

2. DeWolf, P.A. (1971) Electromagnetic reflection from an extended turbulent medium, Cumulative forward-scatter single-backscatter approximation, IEEE Trans. Antennas Propag. AP 19:254.

integrals. For Gaussian correlation functions, the required integrations could be evaluated analytically. This calculation was carried out in I.

Many measurements of ionospheric irregularity fluctuation spectra[3,4,5] support some form of power law for the fluctuation spectrum and for such power law spectra, the convolution integrals cannot, in general, be evaluated analytically. Therefore, one objective of this report will be to evaluate multiple scattering cross sections for fluctuation spectra that cannot be convolved analytically and for the three-dimensional Kolmogoroff spectrum in particular. We will also extend the cross section calculation in I to include scattering into forward directions and scattering from slabs containing irregularities whose symmetry axes are oriented at an arbitrary angle with respect to the slab face.

2. CROSS SECTION FOR FORWARD SCATTERING

The only formal difference between the calculation of scattering into forward directions and scattering into backward direction lies in changing the path length for the scattered wave as it appears in Eq. I-45. Thus, the expression for the backward-path length $x\beta_f$ should be replaced by the path length $(L-x)\beta_f$ which represents the path length from the scatter site on the plane located x units of length from the front of the slab to the back of the slab at L. Integrating over the volume of the slab yields the analog of Eq. (I-46).

$$A \int_0^L dx \, e^{x\beta_i [D_i(\Delta \vec{r})-1] + [L-x]\beta_f \, D_f(\Delta \vec{r})-1]}$$

$$*[AL] \; \frac{e^{L\beta_i [D_i(\Delta \vec{r})-1]} - e^{L\beta_f [D_f(\Delta \vec{r})-1]}}{L\beta_i [D_i(\Delta \vec{r})-1] - L\beta_f [D_f(\Delta \vec{r})-1]} \quad (1)$$

3. Erukhimov, L. M., Kosolapenko, V. I., Lerner, A. M., and Myasnikov, E. N.. (1982) Form of the inhomogeneity spectrum of the high-latitude ionosphere in the direction of the geomagnetic field, Radio Phys. Quart. Electronics 24:350.

4. Kelley, M. C., Livingston, R. C., Rino, C. L., and Tsunoda, R. T. (1982) The vertical wave number spectrum of topside equatorial spread F: Estimates of backscatter levels and implications for a unified theory, J. Geophys. Res. 87(A7):5217.

5. Ossakow, S. L. (1979) Ionospheric irregularities, Rev. Geophys. Space Phys. 17:521.

To expand this as a double functional Taylor series in $D_i(\vec{\Delta r})$ and $D_f(\vec{\Delta r})$, we first define $v_i = L\beta_i \, D_i(\vec{\Delta r})$, $c_i = L\beta_i$ and an equivalent v_f, c_f with the subscript f replacing i. The Taylor expansion is then given by

$$[AL] \sum_{n=0}^{\infty} \left[v_i \frac{\partial}{\partial v_i} + v_f \frac{\partial}{\partial v_f} \right]^n \frac{1}{n!} \frac{e^{v_i - c_i} - e^{v_f - c_f}}{[(v_i - c_i) - (v_f - c_f)]}_{v_i, v_f = 0} \tag{2}$$

Expanding the bracket using the binomial theorem yields

$$[v] \left\{ \frac{e^{-c_i} - e^{-c_f}}{-(c_i - c_f)} + \sum_{n=1}^{\infty} \sum_{j=0}^{n} \frac{1}{n!} \frac{n!}{(n-j)! \, j!} \right.$$

$$\left. \cdot v_i^{n-j} v_f^{j} \left[\frac{\partial^{n-j}}{\partial v_i^{n-j}} \frac{\partial^j}{\partial v_f^i} \left(\frac{e^{v_i - c_i} - e^{v_f - c_f}}{[(v_i - c_i) - (v_f - c_f)]} \right) \right]_{v_i, v_f = 0} \right\} \tag{3}$$

Writing $v_- = v_i - v_f$ and $c_- = c_i - c_f$, the derivative term may be rewritten as

$$\frac{\partial^j}{\partial v_f^j} \left[e^{v_f - c_f} \left[\frac{\partial^{n-j}}{\partial v_i^{n-j}} \left(\frac{e^{v_- - c_-} - 1}{(v_- - c_-)} \right) \right] \right]_{v_i, v_f = 0}$$

$$= \sum_{k=0}^{j} \binom{j}{k} \frac{\partial^{j-k}}{\partial v_f^{j-k}} \left[e^{v_f - c_f} \right] \frac{\partial^k}{\partial v_f^k} \left[\frac{\partial^{n-j}}{\partial v_i^{n-j}} \left(\frac{e^{v_- - c_-} - 1}{v_- - c_-} \right) \right]_{v_i, v_f = 0}$$

$$= \sum_{k=0}^{j} \frac{j!}{(j-k)! \, k!} e^{-c_f} (-1)^k \left[\frac{\partial^{n-j+k}}{\partial v_-^{n-j+k}} \left[\frac{e^{v_- - c_-} - 1}{v_- - c_-} \right] \right]_{v_- = 0}. \tag{4}$$

Using the result of Eq. (I-53), this may be re-expressed as

$$\sum_{k=0}^{j} \frac{j!}{(j-k)! \, k!} e^{-c_f} (-1)^k \frac{\gamma(n-j+k+1, \, c_i - c_f)}{(c_i - c_f)^{n-j+k+1}}. \tag{5}$$

3

Comparing Eqs. (3) and (5) with Eq. (I-54) shows that scattering into the forward direction will be given by Eq. (I-54)

with

$$\left[\frac{e^{-\beta_f L} - e^{-\beta_i L}}{(\beta_i - \beta_f) L} \right] \qquad (6)$$

replacing

$$\left[\frac{1 - e^{-(\beta_i + \beta_f) L}}{(\beta_i + \beta_f) L} \right] \qquad (7)$$

and

$$\gamma(n + 1, j; (\beta_i - \beta_f) L) = \sum_{k=0}^{j} \frac{j!}{(j-k)! k!} e^{-\beta_f L} (-1)^k \gamma(n-j+1, (\beta_i - \beta_f)L)$$

$$\cdot \left[(\beta_i - \beta_f) L \right]^{j-k} \qquad (8)$$

replacing

$$\gamma(n + 1, (\beta_i + \beta_f)L). \qquad (9)$$

In calculating cross sections thus far, we have assumed that $k_o L_o \gg 1$ where L_o is the smaller of the inertial scale lengths ($L_{\parallel}$, $L_{\perp}$), and that the cumulative forward-scatter single-backscatter (CFSB) approximation holds. This is a good approximation for scattering into backward directions. However, for forward directions, it is possible that double and higher order scattering with angles larger than $\theta_c = 1/k_o L_o$ may contribute appreciably to the cross section. DeWolf has calculated that, for a single back scattering, the ratio of scattered intensity outside a cone of half angle θ_D to the intensity inside the cone $I(\theta > \theta_D)/I(\theta < \theta_D)$ is approximately given by $(2k_o L_o \sin \theta_D/2)^{-5/3}$. If this ratio is still small for forward directions, the single scatter CSFB approximation should be adequate. As an example, if we require this ratio to be no greater than 10^{-2}, this would imply, for the choices of $K_o = 8\pi$, $L_o = 2.0$ and $\theta_c = (K_o L_o)^{-1} = 1.14°$, that $\theta_D = 18.1°$. Thus we should be reasonably safe in pressing the CFSB into within, say, 36° of the forward scattering direction for this choice of parameters.

4

Comparing Eqs. (3) and (5) with Eq. (I-54) shows that scattering into the forward direction will be given by Eq. (I-54)

with
$$\left[\frac{e^{-\beta_f L} - e^{-\beta_i L}}{(\beta_i - \beta_f) L} \right] \tag{6}$$

replacing
$$\left[\frac{1 - e^{-(\beta_i + \beta_f) L}}{(\beta_i + \beta_f) L} \right] \tag{7}$$

and
$$\gamma(n + 1, j; (\beta_i - \beta_f) L) = \sum_{k=0}^{j} \frac{j!}{(j-k)!k!} e^{-\beta_f L} (-1)^k \gamma(n-j+1, (\beta_i - \beta_f)L)$$
$$\cdot \left[(\beta_i - \beta_f) L \right]^{j-k} \tag{8}$$

replacing
$$\gamma(n + 1, (\beta_i + \beta_f)L). \tag{9}$$

In calculating cross sections thus far, we have assumed that $k_o L_o \gg 1$ where L_o is the smaller of the inertial scale lengths ($L_{\parallel}$, $L_{\perp}$), and that the cumulative forward-scatter single-backscatter (CFSB) approximation holds. This is a good approximation for scattering into backward directions. However, for forward directions, it is possible that double and higher order scattering with angles larger than $\theta_c = 1/k_o L_o$ may contribute appreciably to the cross section. DeWolf has calculated that, for a single back scattering, the ratio of scattered intensity outside a cone of half angle θ_D to the intensity inside the cone $I(\theta > \theta_D)/I(\theta < \theta_D)$ is approximately given by $(2k_o L_o \sin \theta_D/2)^{-5/3}$. If this ratio is still small for forward directions, the single scatter CSFB approximation should be adequate. As an example, if we require this ratio to be no greater than 10^{-2}, this would imply, for the choices of $K_o = 8\pi$, $L_o = 2.0$ and $\theta_c = (K_o L_o)^{-1} = 1.14°$, that $\theta_D = 18.1°$. Thus we should be reasonably safe in pressing the CFSB into within, say, 36° of the forward scattering direction for this choice of parameters.

4

3. KOLMOGOROFF SPECTRUM OF TURBULENCE

The choice of a Gaussian spectrum of turbulence in I made it possible for all convolution integrations, such as that in Eq. (I.61) to be evaluated analytically. For power law spectra and spectra having more complex functional forms, numerical integration will generally be required. For these cases, a further distinction may be made depending on whether or not the projected correlation functions to be convolved in the k_x-k_y plane can be transformed into functions having circular symmetry. For functions that can be represented this way, the cross section calculation may be structured so that the set of multiple convolutions of the projected correlation function $\left\{ \breve{D}_i^n (\vec{k}) \right\}$ become independent of X_i and need to be calculated only once; the X_i and X_f dependence is thus transferred to another, simpler part of the integration. For correlation functions that cannot be transformed to circular symmetry, numerical evaluation is more costly, since the set of projected correlations $\left\{ \breve{D}_i^n (\vec{k}) \right\}$ will, in general, depend on X_i as well as on k_x and k_y separately.

Since our main concern is in studying the effects of multiple scattering from physically realizable turbulence, we will concentrate on spectra having the power law form given by Eq. (10).

$$\widetilde{\phi}^{3d}(\vec{k}) = \frac{\kappa_3}{\left[1 + \vec{k}_\perp^2 L_\perp^2 + k_z^2 L_\parallel^2 \right]^{1+\nu}} \tag{10}$$

where

$$\kappa_3 = 4\pi^2 \frac{L_\parallel L_\perp^2 \Gamma(\nu+1)}{\Gamma(3/2) \Gamma(\nu-1/2)} \tag{11}$$

is the normalization constant for $\widetilde{\phi}^{3d}(\vec{k})$ defined by the condition $\phi^{3d}(\vec{r}=0) = 1$.

For such spectra, analytic evaluation is a reasonable possibility, but only if ν equals an integer or half integer. For ν, an integer or half integer the convolution integrals may be evaluated straightforwardly by contour integration. However, even for the simplest case of $\nu = 1$, the proliferation of terms for higher order convolutions makes this a tedious procedure. For the Kolmogoroff spectrum with $\nu = 5/6$, the convolution integrations are best carried out numerically. To accomplish this, we suggested in I representing the Kolmogoroff spectrum as a sum of Gaussians. This allows all of the convolution integrals to be evaluated analytically, yielding a new sum of Gaussians as the result. Upon trying this approach, however, we found that the series converged slowly, and that such a large number of terms was needed to represent the Kolmogoroff spectrum adequately that no advantage could be gained over direct numerical integration.

To evaluate the convolution integrals for the cross section [Eq. (I.54)] most efficiently, it is advantageous, as pointed out in I, to use the delta function projection operators appearing in the projected correlation functions $\widetilde{D}_{i,f}$ [Eq. (I.39)] to integrate out the z components of momentum. The resulting convolution integrations are then confined to the k_x, k_y plane. Using the results of the theorem proved in I (Appendix C), all convolutions of the projected correlation function based on Eq. (10) such as

$$\widetilde{D}_i^n(\vec{k}) = \int \frac{d^3k'}{(2\pi)^3} \, \widetilde{D}_i^{n-1}(\vec{k}-\vec{k}') \, \widetilde{D}_i(\vec{k}') \tag{12}$$

may be written in the k_x, k_y plane as

$$\breve{D}_i^n(k_1^2\ell_i^2, k_2^2) = \int \frac{d\vec{k_1'}}{(2\pi)^2} \, \breve{D}_i^{n-1}((k_1-k_1')^2 \ell_i^2, (k_2-k_2')^2) \breve{D}_i(k_1'^2\ell_i^2, k_2'^2) \tag{13}$$

where

$$\ell_i^2 = 1 + \eta^2 \tan^2(X_i), \quad \eta = L_{\parallel}/L_{\perp}, \tag{14}$$

and where $\breve{D}_i(\vec{k})$ is defined through the relation [Eq. (I.56)]

$$\widetilde{D}_i(\vec{k}) = \breve{D}_i(\vec{k}_\perp) \, \delta(\vec{k} \cdot \vec{K}_i) \, 2\pi K_z \tag{15}$$

as

$$\breve{D}_i(\vec{k}_\perp) = \breve{D}_i(k_1^2 \ell_i^2, k_2^2) = \widetilde{\phi}_i^{2d}(k_1\ell_i, k_2) = \frac{\kappa_{2i}}{[1 + k_1^2(\ell_i L_\perp)^2 + k_2^2 L_\perp^2]^{1+\nu}} \tag{16}$$

with

$$\kappa_{2i} = 4\pi(L_\perp \ell_i)L_\perp \nu. \tag{17}$$

The normalization constant κ_{2i} is defined by the condition that $\phi^{2d}(\vec{r}_\perp = 0) = 1$ which yields Eq. (17) when used with scale lengths $L_1 = \ell_i L_\perp$, $L_2 = L_\perp$. The path dependent attenuation constant α_{X_i}, defined through the relation [Eq. (I.39)], is given by

6

$$\alpha_{\chi_i} = \frac{K^2 \ \delta\epsilon^2 \ \kappa_3 \cdot 3}{40(2\pi)\ell_i L_\perp \cos(\chi_i)} . \tag{18}$$

In terms of dimensionless variables $\vec{p}_\perp = \vec{k}_\perp L_\perp$ Eq. (13) may be re-expressed as

$$\breve{D}_i^n (p_1^2 \ell_i^2, \ p_2^2) = \frac{1}{L_\perp^2} \int \frac{d\vec{P}_\perp'}{(2\pi)^2} \ \breve{D}_i^{n-1}((p_1-p_1')^2 \ell_i^2, \ (p_2-p_2'^2))\breve{D}_i(p_1'^2 \ell_i^2, p_2'^2). \tag{19}$$

By rescaling the p_1 momentum coordinate, we can rewrite Eq. (19) as a two-dimensional convolution of circularly symmetric functions. Thus, with the coordinate transformation

$$P_1 = p_1 \ell_i, \ P_2 = p_2 \tag{20}$$

and defining

$$\breve{D}_i(\vec{P}_\perp) = \frac{\kappa_{2i}}{[1+\vec{P}_\perp^2]^{1+\nu}} = \frac{\kappa_{2i}}{[1+p_2^2 + p_1^2 \ell_i^2]^{1+\nu}} = \breve{D}_i(\vec{p}_\perp) \tag{21}$$

we have

$$\overset{\cup}{D}_i^n(\vec{P}_\perp) = \frac{\breve{D}_i^n(\vec{p}_\perp)}{(\ell_i L_\perp^2)^{n-1}} \tag{22}$$

The multiple convolution products for the scaled projected correlation function will then be given by

$$\overset{\cup}{D}_i^n(\vec{P}_\perp^2) = \int \overset{\cup}{D}_i^{n-1}((\vec{P}_\perp - \vec{P}_\perp')^2) \ \breve{D}_i(\vec{P}_\perp'^2) \ \frac{d\vec{P}_\perp'}{(2\pi)^2} \tag{23}$$

Using the results of the Appendix for convolving two circularly symmetric functions, Eq. (23) may be written equivalently as

$$\overset{\cup}{D}_i^n(P_\perp^2) = \int_0^\infty \int_0^{2\pi} \overset{\cup}{D}_i^{n-1}(P_\perp^2 + Q_\perp^2 - 2P_\perp Q_\perp \cos(\phi_Q))\breve{D}_i(Q^2)\frac{Q_\perp dQ_\perp d\phi_Q}{(2\pi)^2} \tag{24}$$

7

$$= \frac{1}{(2\pi)^2} \int_0^\infty \frac{dQ^2}{2} \int_{Q'^2 = (Q-P)^2}^{Q'^2 = (Q+P)^2} \frac{\breve{D}_i^{n-1}(Q^2)\breve{D}_i(Q'^2)\, dQ'^2/2}{[(Q+P)^2 - Q'^2]^{1/2}[Q'^2 - (Q-P)^2]^{1/2}} \quad (25)$$

or

$$= \int_0^\infty Q\,dQ \int_0^\infty \frac{Q'dQ'}{(2\pi)^2} \breve{D}_i^{n-1}(Q^2)\, \breve{D}_i(Q'^2) \frac{\Delta(Q + Q' - P)}{A} \quad (26)$$

where $\Delta(Q + Q' - P) = 1$ if Q, Q', and P form the sides of a triangle of area A and zero otherwise.

By making the coordinate transformation given by Eq. (20), integration of a general term such as Eq. (I-60) can be re-expressed as

$$\iint \frac{d\vec{k}}{(2\pi)^6}\, d\vec{k}'\quad \widetilde{D}_i^{n-j}(\vec{k}) < \delta\epsilon^2(\vec{k} - \vec{k}' - \vec{K}_i + \vec{K}_f) > \widetilde{D}_f^j(\vec{k}') \quad (27)$$

$$= \iiiint_{-\infty}^\infty \frac{dp_1 dp_2 dq_1 dq_2}{(L_\perp)^4 (2\pi)^4}\, \breve{D}_i^{n-j}(\vec{p}_\perp) < \delta\epsilon^2(\vec{p} - \vec{q} - \vec{K}_i + \vec{K}_f) > \breve{D}_f^j(\vec{q}_\perp)\Big|_{\substack{p_z = -\frac{\vec{p}_\perp \cdot \vec{K}_{i\perp}}{K_{iz}}, \\ q_z = \frac{\vec{q}_\perp \cdot \vec{K}_{f\perp}}{K_{fz}}}}$$

$$= \iiiint_{-\infty}^\infty \frac{dP_1\, dP_2\, dQ_1\, dQ_2}{\ell_i\, \ell_f\, (L_\perp)^4 (2\pi)^4}\quad \frac{\breve{D}_i^{n-j}(\vec{P}_\perp)}{\ell_i^{n-j-1}}\quad \frac{\breve{D}_f^j(\vec{Q}_\perp)}{\ell_f^{j-1}(L_\perp^2)^{n-2}}$$

$$\cdot < \delta\epsilon^2(\frac{P_1}{\ell_i},\ P_2,\ \frac{Q_1}{\ell_f},\ Q_2,\ \vec{K}_i,\ \vec{K}_f) > .$$

The X_i and X_f dependence of the integrand has thus been transferred from the arguments of $\breve{D}_i^{n-j}$ and $\breve{D}_f^j$, where it appeared in the form of the scale factors ℓ_i and ℓ_f, to the term $< \delta\epsilon^2 >$. The factors $\ell_i^{-n+j}\, \ell_f^{-j}\, L_\perp^{-2n}$ will be cancelled when account is taken of the terms $\kappa_{2i}^{n-j}\kappa_{2f}^j$ appearing in $\breve{D}_i^{n-j}$. $\breve{D}_f^j$.

For spectral correlation functions that do not lead to circular symmetry in the scaled k_x-k_y plane after integration over the k_z projection delta function, such as the factored ϕ_{KG} of Eq. (I.30) below:

8

$$\tilde{\phi}_{KG}(\vec{k}) = \sqrt{\pi} \quad L_\parallel \ e^{-k^2_z L^2_\parallel /4} \frac{\kappa_2}{[1 + \vec{k}^2_\perp L^2_\perp]^{1+\nu}} \quad , \tag{28}$$

each $\breve{D}^n_i(p_1, p_2)$ will be a function of χ_i and of p_1 and p_2 separately. While the time required to evaluate a look-up table of values for the non-circularly symmetric $\breve{D}_i(p_1, p_2)$ functions is roughly equal to that required for the symmetric ones, the storage requirements will be much larger since the circularly symmetric structure functions $\breve{D}^n_i(P)$ depend only on one variable $P = [P^2_1 + P^2_1]^{1/2}$ (aside from the easily factored dependence on χ_i stemming from κ^n_{2i}).

In the following sections, we shall discuss the results of numerically evaluating the multiscatter cross section for ϕ given by Eq. (10). We have omitted the evaluation of multiscatter cross sections using the mixed representation Eq. (28) simply as a matter of economy. If we neglect multiscatter contributions, however, the attenuated Born cross sections for the Gaussian [Eq. (I.29)], Kolomogoroff [Eq. (10)], and mixed [Eq. (28)] spectral correlation functions can be readily compared and are shown in Figure 1 for transverse and longitudinal scale lengths of $L_\perp = I$, $L_\parallel = 4$ and wavelength $\lambda = 1$ for $\chi_i = 45°$. At the angle for specular backscattering $\chi_f = 135°$, we have $\Delta K_z = 0$. Thus, the magnitude of the backscattering peak will be controlled by the magnitude of $\Delta K_\perp \cdot L_\perp$ and the overall Rayleigh $(2\pi/\lambda)^4$ factor. A change in wavelength from $\lambda = 1$ to $\lambda = 1/2$ will entail an approximate 25 orders of magnitude decrease in the Gaussian cross section, whereas the two Kolomogoroff cross sections are virtually unchanged due to the K^4 Rayleigh prefactor increase balancing the $(1 + \Delta K^2_\perp L^2_\perp)^{1+5/6}$ denominator increase. In the forward direction, both ΔK_z and $\Delta K_\perp$ are zero, and the peak cross section values are determined by the Rayleigh K^4 behavior.

4. SLAB GEOMETRY

In I, the symmetry axis of the irregularities was chosen to be parallel to the face of the slab. It is a straightforward matter to modify the cross section calculation to account for a geometry having the irregularities aligned at an arbitrary angle with respect to the face of the slab.

For the general case shown in Figure 2, we start from the situation of a horizontal slab with irregularities aligned perpendicular to the slab face and then define a tilt angle α that defines the rotation of the symmetry axis of the irregularities in the xz plane away from the z axis, and a rotation angle β that defines the rotation of the projection of the irregularity in the xy plane clockwise from the
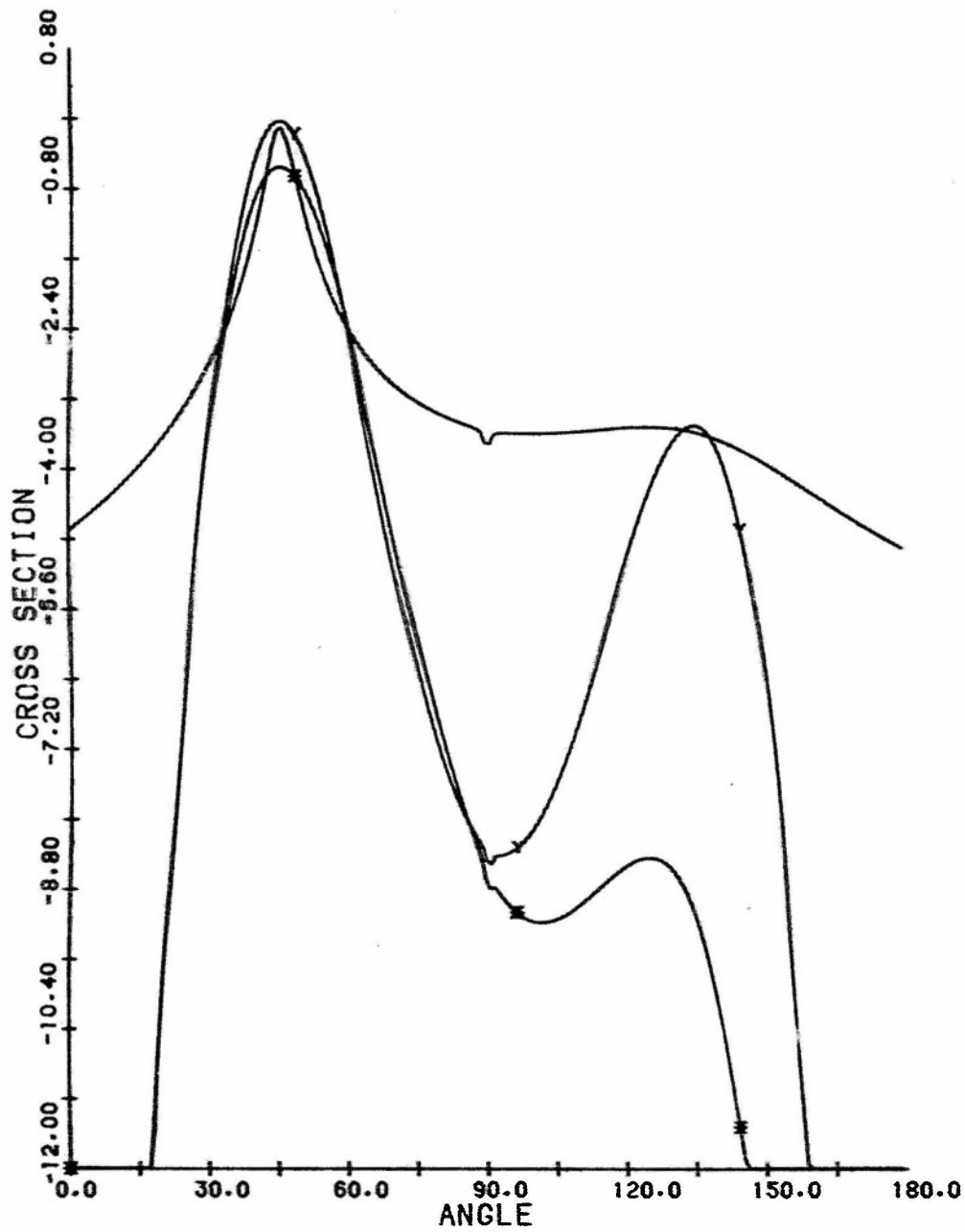
9

Figure 1. Logarithmic Plot of Attenuated Born Cross Sections vs χ_f for the Gaussian (*), Kolmogoroff, and Mixed Correlation Functions (γ) With $K = 2\pi$, $L = 1$, $\eta = 4$, $\delta\epsilon = 0.01$
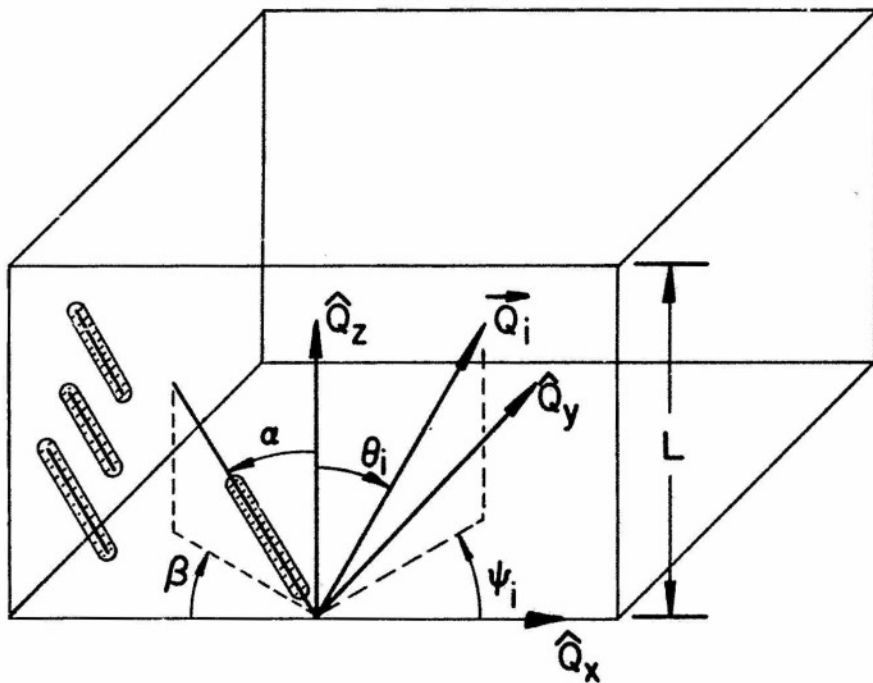
10

Figure 2. Geometry of Scattering Angles With Respect to a Fixed Slab
With Rotated Irregularities

x axis. The path length factor $s_i(x)^*$ will now be replaced by

$$s'_i(z) = \frac{z}{|\cos(\theta_i)|} \tag{29}$$

with z measuring distance into the slab. The path-dependent attenuation and the
scattering cross section can now be found by expressing the wave vector components

---

* In I, the angle X in Figure A1 was mislabeled. It should be the angle ACD
  yielding an expression for the path length Eq. (I.43) $s(x) = x/|\cos(\phi)\sin(X)| =$
  AC. (This will not entail a change in the numerically computed curves in I
  as $\phi_{i,f}$ was taken to be 0 or π for all cases).

11

parallel (K_3) and perpendicular ($K_{1,2}$) to the irregularities in terms of two coordinate rotations through angles α and β.

Thus we have

$$K_1 = Q_1' \cos \alpha + Q_3' \sin \alpha$$

$$K_2 = Q_2'$$

$$K_3 = -Q_1' \sin \alpha + Q_3' \cos \alpha \tag{30}$$

with

$$Q_1' = Q_x \cos \beta - Q_y \sin \beta$$

$$Q_2' = Q_x \sin \beta + Q_y \cos \beta$$

$$Q_3' = Q_z$$

where $\{Q_x, Q_y, Q_z\} = \{K \sin(\theta) \cos(\psi), K \sin(\theta) \sin(\psi), K \cos(\theta)\}$ are the components of the wave vector with respect to the slab with rotated irregularities, and $\{K_1, K_2, K_3\} = \{K \sin(\chi) \cos(\phi), K \sin(\chi) \sin(\phi), K \cos(\chi)\}$ are the components of $\vec{Q}_i$ or $\vec{Q}_f$ with respect to the irregularity. The steps required to determine $\sigma_{\vec{Q}_i \vec{Q}_f}(\alpha, \beta)$ for the general case of scattering from a horizontal slab with rotated irregularities are: (1) for given $\vec{Q}_i$ and $\vec{Q}_f$, use Eq. (30) to find the corresponding $\vec{K}_i$ and $\vec{K}_f$; (2) use the results of Eq. (I.40) to find $\alpha_{\chi_i}[\vec{Q}_i]$ and $\alpha_{\chi_f}[\vec{Q}_f]$; (3) according to whether $\vec{Q}_i$ and $\vec{Q}_f$ are on opposite sides or the same side of the slab, use [along with 5.1 for $s'_{i,f}(z)$] Eqs. (6) and (8) or Eqs. (7) and (9) for the attenuation and γ factors; (4) determine

$$\sigma_{\vec{Q}_i, \vec{Q}_f}(\alpha, \beta) = \sigma_{\vec{K}[Q_i] \vec{K}_f[Q_f]}(\alpha_{\chi_{i, f}}[\vec{Q}_{i, f}], \gamma[\vec{Q}_{i, f}]). \tag{31}$$

As an example of the effect of rotating the irregularity axis on the multiple scattering cross section, we take $\beta = 0$ and evaluate $\sigma_{\vec{Q}_i, \vec{Q}_f}$ for various values of α for the Kolmogoroff spectrum. Assuming that initial and final wave vector are confined to the $\phi = 0$ (x-z) plane, we may redefine the ranges of $\chi_{i, f}$ and $\theta_{i, f}$ to extend to $\pm 2\pi$.

In this plane, we then have the relation

$$X_i = \alpha + \theta_i \tag{32}$$

and

$$X_f = \alpha + \theta_f \ .$$

as shown in Figure 3.

For specular scattering $\pi - X_i = X_f - \pi$ and from Eq. (32), this implies

$$\theta_f = -2\alpha - \theta_i. \tag{33}$$

For $\theta_i = 45°$ and for values of $\alpha = 0°$, $30°$, $60°$ and $90°$, this yields expected outgoing angles for spectral scattering of $\theta_f = 315°$, $255°$, $195°$, and $135°$ respectively.
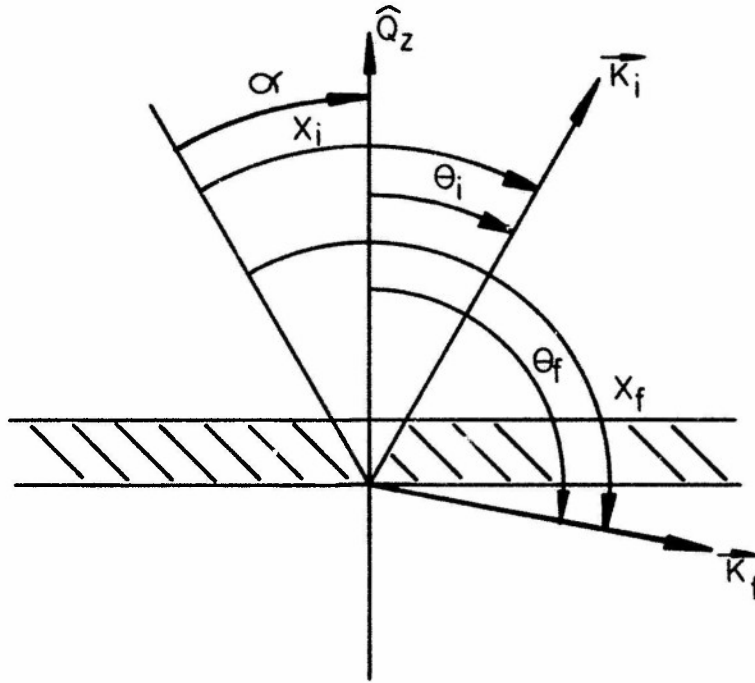

Figure 3. Geometry of Scattering Angles With Respect to a Fixed Slab With Rotated Irregularity Axes for $\beta = 0$

In Figure 4, we have plotted the total cross section $\sigma_{\vec{Q}_i, \vec{Q}_f}(\alpha, \beta = 0)$ vs θ_f for values of $\alpha = 0°$, $30°$, $60°$, and $90°$ for a slab with $L = 1$, $\eta = L_{\parallel}/L_{\perp} = 4$ with $K = 4\pi$ for Kolmogoroff turbulence. The spectral peaks appear close to their expected values. While there will be narrow ranges near $\theta_f = 90°$ and $270°$ where the cross section will vanish due to attenuation in an effectively infinite slab, the decrease in $\sigma_{\vec{Q}_i, \vec{Q}_f}$ for the ranges of approximately $\pm 10°$ on either side of these grazing angles does not show up. This is caused by a near cancellation between the attenuation of the Born term and the added contribution of multiscatter terms with $n \geq 1$ as can be seen in Figure 5 where the two contributions are plotted separately.

5. NUMERICAL RESULTS FOR MULTISCATTER CROSS SECTIONS

In this section, we present numerical results of multiple scattering cross sections as a function of the polar angle X_f for various values of $\eta = \dfrac{L_{\parallel}}{L_{\perp}}$, L, K, and X_i. These results extend the calculations of I to forward directions as discussed in Section 2 and to the case of the Kolmogoroff spectrum as discussed in Section 3. For all cases considered, we assume scattering from a slab of irregularities with the long axis of the irregularities parallel to the slab face ($\alpha = 90°$ $\beta = 0$). In keeping with the angle designations of I, we shall plot cross sections vs X_f. For purposes of displaying results, we define X_f to be negative in the forward direction, $X_f = -|X_f|$ for $\phi_f = 0$.

In Figures 6 and 7, the logarithm of the total scattering cross section σ_{X_i, X_f} is plotted vs X_f for the Kolmogoroff and Gaussian spectral functions respectively. In the forward direction, the Kolmogoroff cross section is seen to satisfy the requirements of the forward scatter approximation better than the Gaussian in that the cross section falls off much more rapidly as $|X_f - X_i|$ increases. Around the specular backscattering peak, it is the Gaussian cross section that falls off most rapidly as a function of X_f. This behavior can be readily understood in terms of the derivatives of the corresponding spectral functions.

$$\frac{\partial}{\partial X_f} \ln \Phi_G = -\frac{K}{2} \left\{ \Delta K_{\perp} \cos(X_f) \cos(\phi_i - \phi_f) L_{\perp}^2 - \Delta K_{\parallel} \sin(X_f) L_{\parallel}^2 \right\} \quad (34)$$

$$\frac{\partial}{\partial X_f} \ln \Phi_K = -\frac{K}{(1+\nu)} \frac{\left\{ \Delta K_{\perp} \cos(X_f) \cos(\phi_i - \phi_f) L_{\perp}^2 - \Delta K_{\parallel} \sin(X_f) L_{\parallel}^2 \right\}}{\left\{ 1 + \Delta K_{\perp}^2 L_{\perp}^2 + \Delta K_{\parallel}^2 L_{\parallel}^2 \right\}} \quad (35)$$

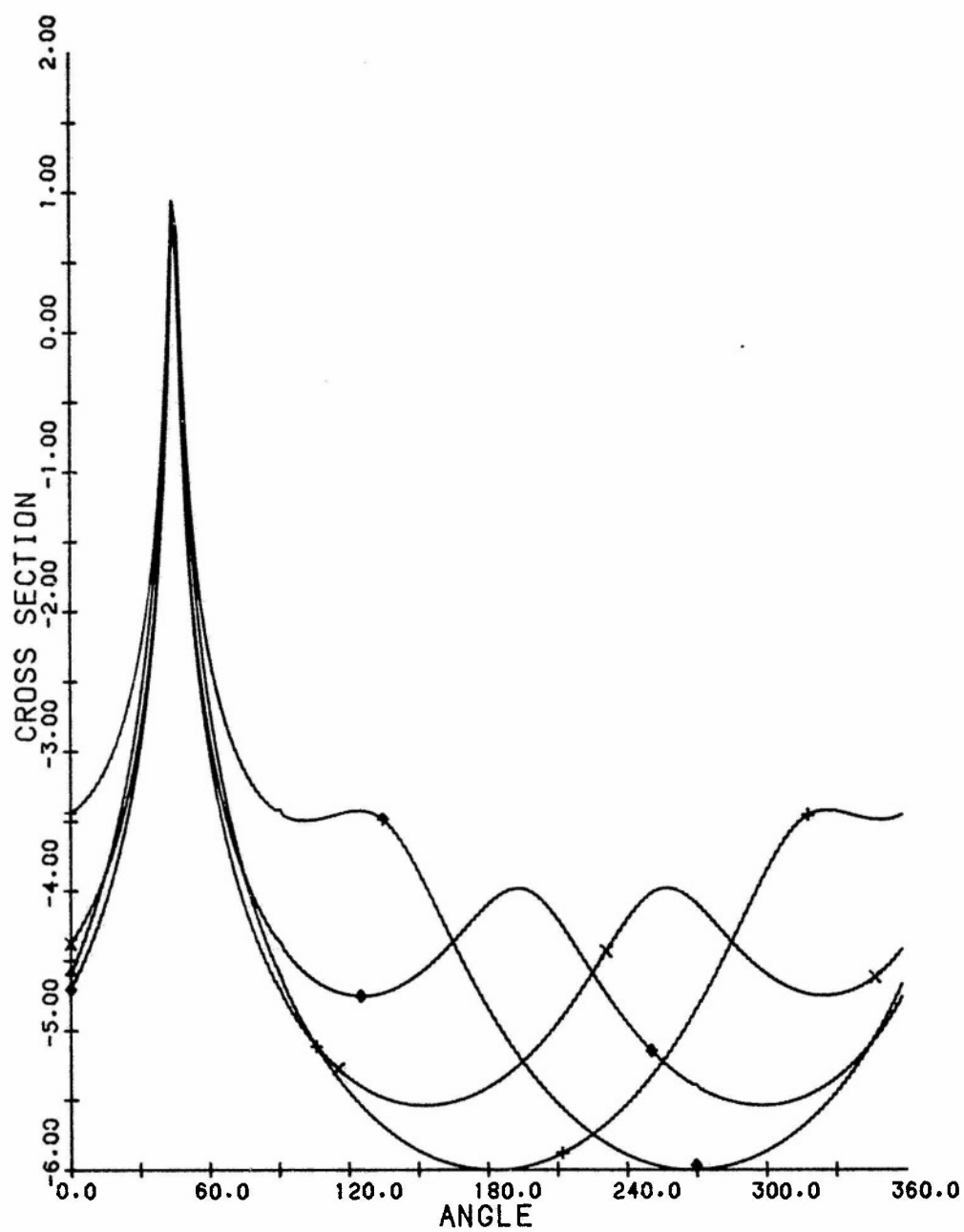In the forward direction, $\Delta K_{\perp}$ is small, $\Delta K_{\parallel} = 0$, and the slope of the

14

Figure 4. Logarithmic Plot of Total Cross Section vs θ_f for Irregularity Tilt Angle $\alpha = 0°$ (+), $\alpha = 30°$ (x), $\alpha = 60°$ (◊), and $\alpha = 90°$ (♦) With $K = 4\pi$, $L = 1$, $\eta = 4$, $\delta\epsilon = 0.01$
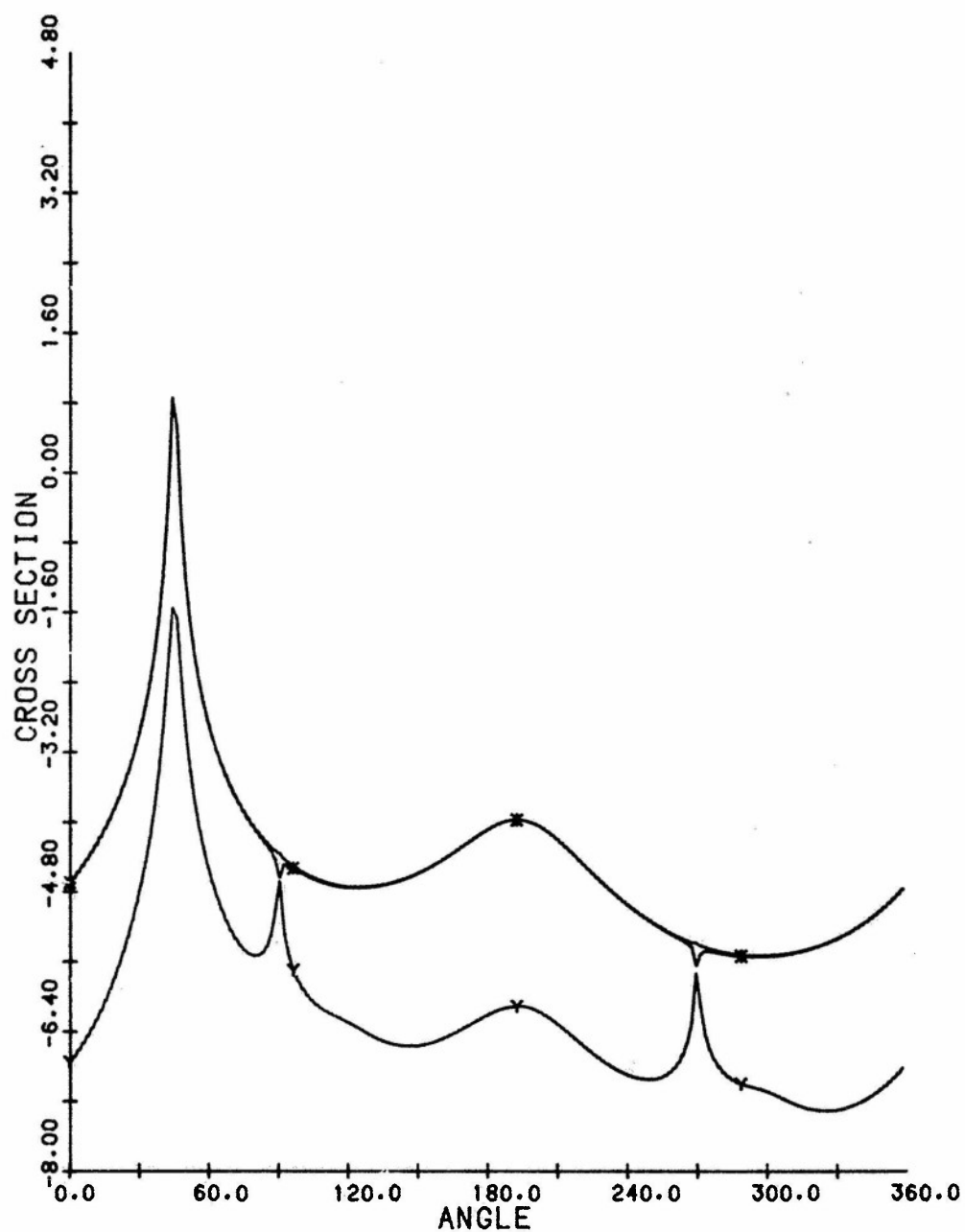
15

Figure 5.   Logarithmic Plot of Born (*), Multiscattering (γ), and Total Cross Sections vs χ_f for Irregularity Tilt Angle $\alpha = 60°$ With K = 4π, L = 1, $\eta = 4$, $\delta\epsilon = 0.01$
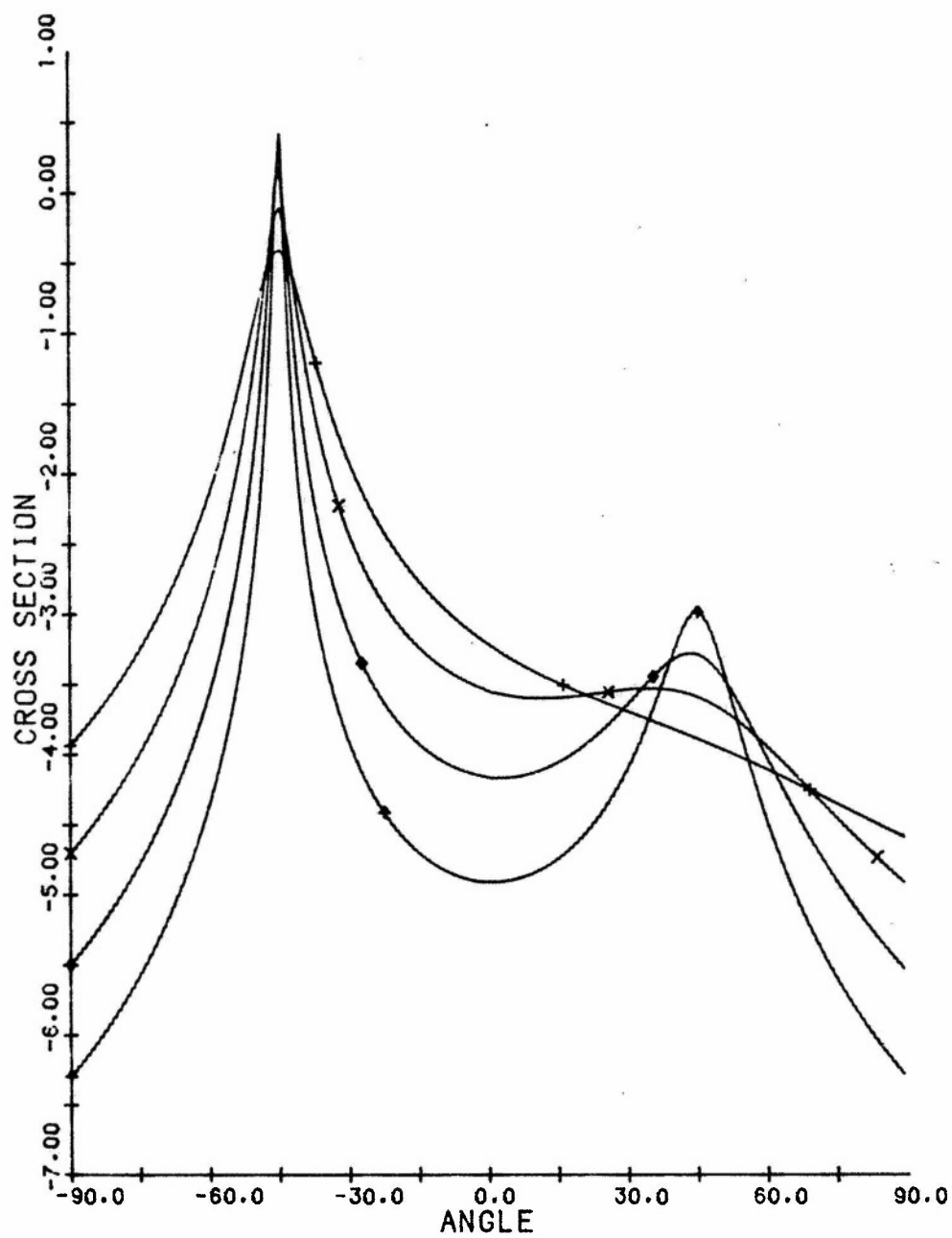
16

Figure 6. Logarithmic Plot of Total Cross Sections vs χ_f for Kolmogoroff Turbulence for $\eta = 2(+)$, $\eta = 4(x)$, $\eta = 8(\Diamond)$, and $\eta = 16(\phi)$ With $K = 2\pi$, $L = 1$, $\delta\epsilon = 0.01$
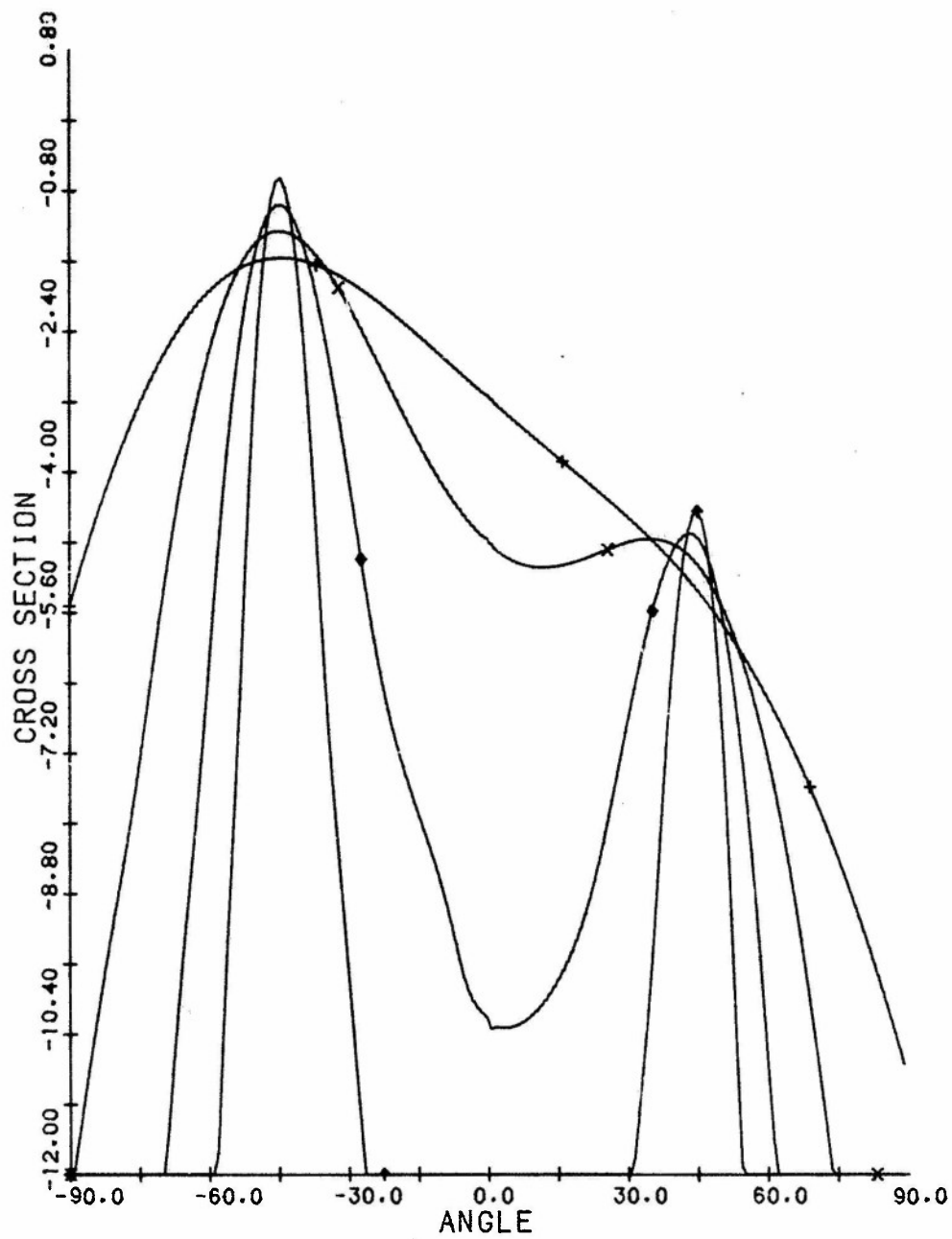
17

Figure 7. Logarithmic Plot of Total Cross Sections vs X_f for Gaussian Turbulence for $\eta = 2(+)$, $\eta = 4(x)$, $\eta = 8(\Diamond)$, and $\eta = 16(\dagger)$ With $K = 4\pi/3$, $L = 1.0$, $\delta\epsilon = 0.01$

18

Kolmogoroff curve is approximately four times that of the Gaussian

$$\frac{\partial}{\partial x_f} \ln \phi_K \simeq 2 \cdot (1 + \nu) \frac{\partial}{\partial x_f} \ln \phi_G \quad . \tag{36}$$

The factor in brackets in the numerators of Eqs. (34) and (35) can be rewritten for the backscattering case ($\phi_i = 0$, $\phi_f = \pi$) as

$$[\Delta K_\perp \cos(x_f) L_\perp^2 - \Delta K_{||} \sin(x_f) L_{||}^2] \tag{37}$$

$$= -2K \sin\left(\frac{x_i + x_f}{2}\right) \left[\cos\left(\frac{x_i - x_f}{2}\right) \cos(x_f) L_\perp^2 - \sin\left(\frac{x_i - x_f}{2}\right) \sin(x_f) L_{||}^{\ 2}\right] .$$

For $L_{||}^2 \gg L_\perp^2$, this term will have two zeros, one near $x_f = 0$ and one near the specular direction $x_f = x_i$.

As η is reduced, the peak near the specular direction will move in to lower x_f while the minimum at $x_f = 0$ will move out. At some value of $\eta(8 < \eta < 16$ for the examples shown), the peak and minimum will merge and disappear. This behavior can be seen for both the Kolmogoroff and Gaussian spectra. In the case of the Kolmogoroff spectrum, the extra term in the denominator of Eq. (35) implies that the slope of $\ln \sigma^K$ will be smaller than that for $\ln \sigma^G$ by $2(1+\nu)/[1 + \Delta K_\perp^2 L_\perp^2 + \Delta K_{||}^2 L_{||}^2]$ which is approximately $2(1+5/6)/[1 + 2K^2] \simeq 1/14$ for the parameters of Figure 6.

The equal spacing in the values of the amplitudes at the scattering peaks in Figures 6 and 7 reflects the multiplicative factor $L_{||}$ in the normalization constants for ϕ_G and ϕ_K. Since the increments in $L_{||}$ in Figures 6 and 7 proceed by factors of 2, the increments in σ_K and σ_G at their peaks will be additive in increments of log 2.

In Figures 8 and 9, we have plotted the multiple scattering cross sections for the Gaussian and Kolmogoroff spectra for increasing values of K. For the Gaussian case shown in Figure 8, we have plotted the total cross section for $L=1$, $\eta = 4$, and for K taking values of 1.5π, 2π, 2.5π, 3π, and 3.5π. At the position of the forward peak, since the scattering slab is relatively thin and $\Delta\vec{K} = 0$, the K dependence of the scattering cross section is determined by the Rayleigh K^4 factor. At the backscatter peak, as pointed out in 1, the cross section is dominated by the exponential factor $e^{-(\Delta K_\perp^2 L_\perp^2 + \Delta K_{||}^2 L_{||}^2)/4}$. Thus for $K = 3.5\pi$ the value of the Born contribution to the backscatter peak is 0.17×10^{-23}, while the multiscatter contribution there is 0.18×10^{-22}. Because the CFSB approximation depends on satisfying $KL \gg 1$, the Gaussian spectrum offers little
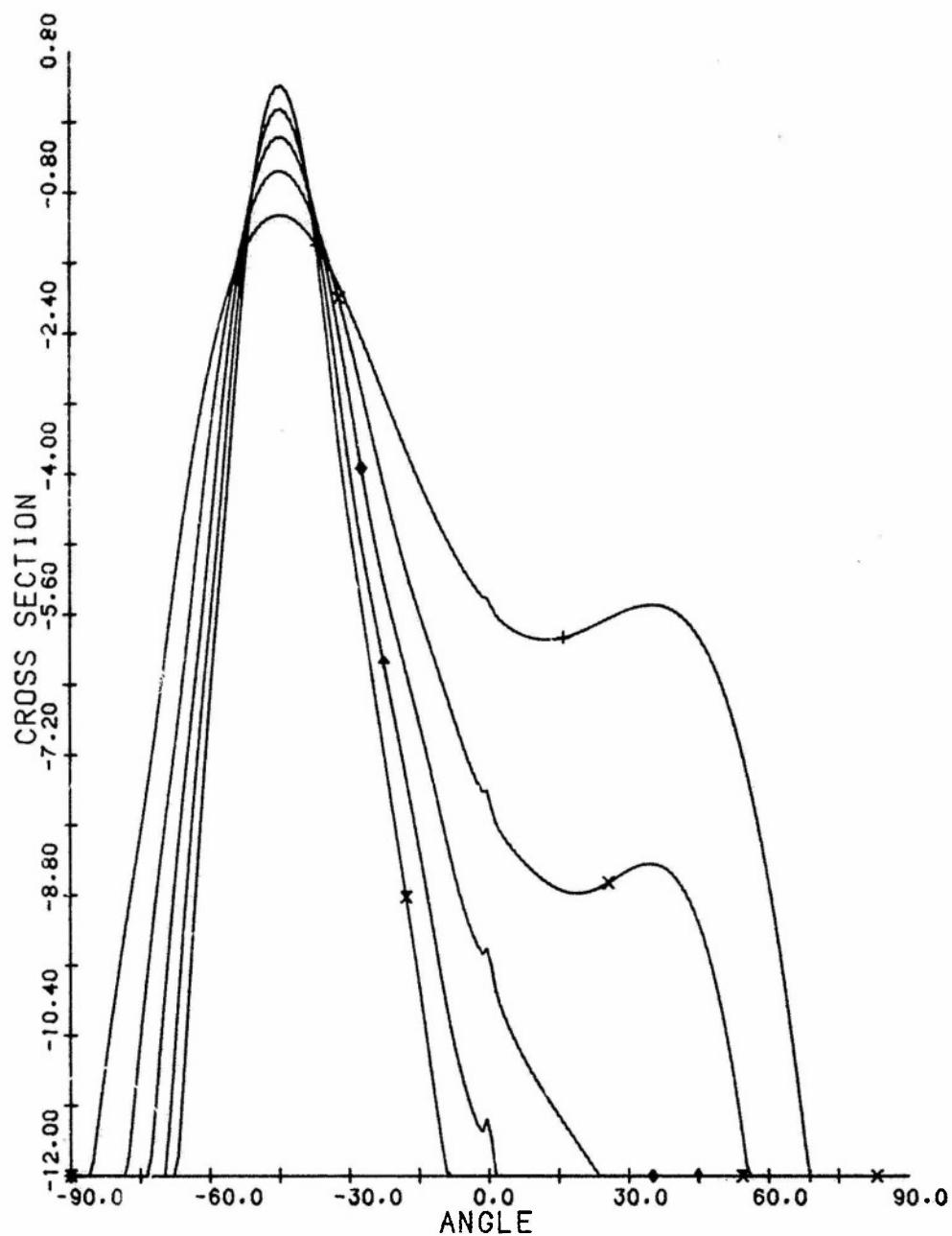
19

Figure 8. Logarithmic Plot of Total Cross Section vs χ_f for Gaussian Turbulence for K = 1.5π(+), K = 2π(x), K = 2.5π(◊), K = 3π($\dagger$), and K = 3.5π($\mathbf{x}$) With η = 4, L = 1.0, $\delta\epsilon$ = 0.01
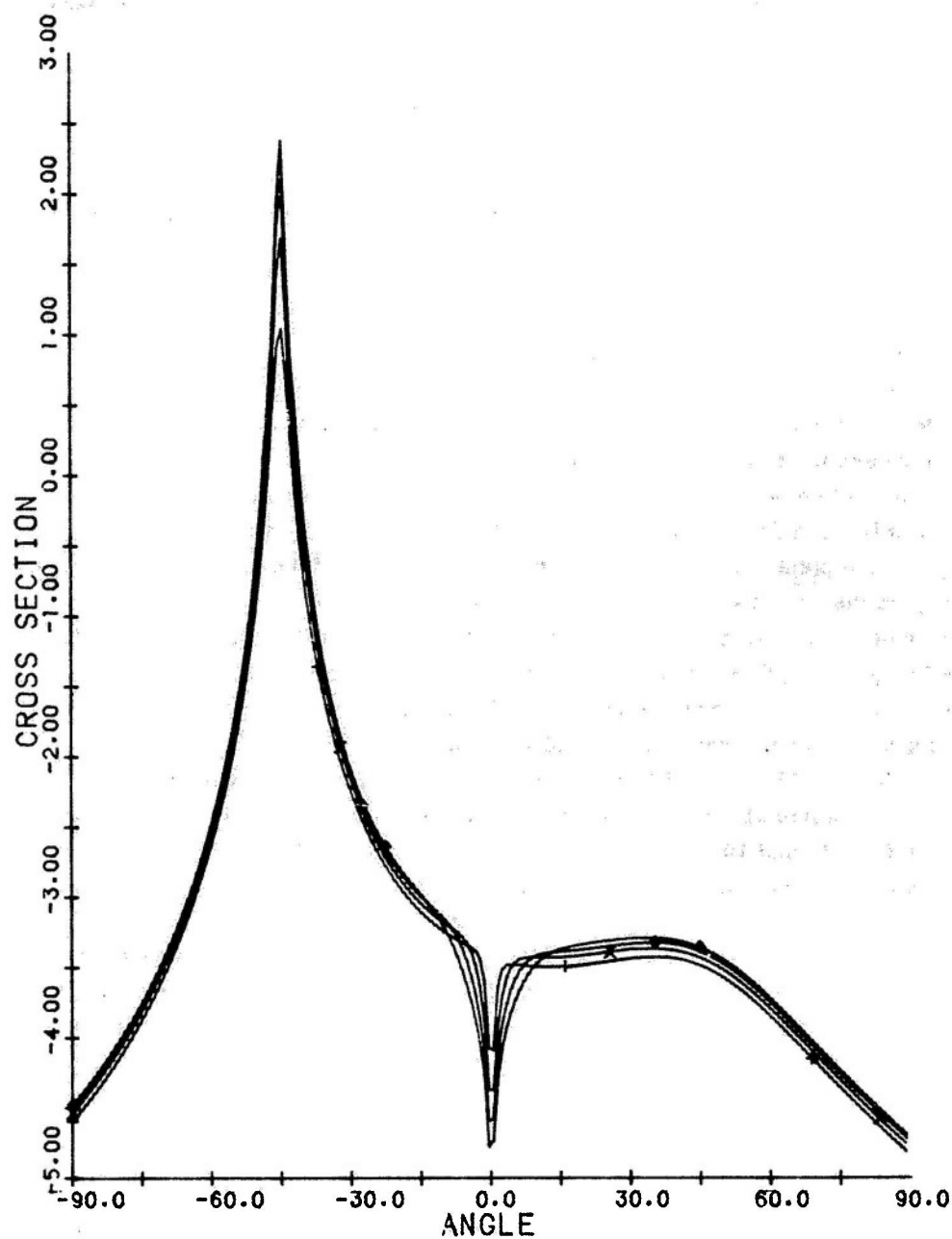
20

Figure 9. Logarithmic Plot of Total Cross Section vs χ_f for Kolmogoroff Turbulence for $K = 4\pi(+)$, $K = 6\pi(\times)$, $K = 8\pi(\lozenge)$, and $K = 10\pi(\blacklozenge)$ With $\eta = 4$, $L = 10$, $\delta\epsilon = 0.01$

21

of interest in the region of specular scattering. The backscatter cross section there for large KL is practically zero.

In Figure 9, we have plotted the total cross section for scattering from Kolmogoroff turbulence with $\eta = 4$, $L = 10$, and for K values of 4π, 6π, 8π, and 10π. For these values of K and L, the forward approximation is adequately satisfied. In the forward direction, the scattering peak is determined by the Rayleigh K^4 factor modified by attenuation because $L=10$ represents a relatively thick scattering slab. At the specular peak near $\chi_f = 40°$, the value of σ_K is seen to change by a relatively small amount as a function of K. For the Born contribution this behavior is caused mainly by $K^4 / [1 + \Delta K_\perp^2 L_i^2]^{1 + 5/6} \sim K^{1/3}$ as K increases (modified by attenuation $e^{-\alpha L}$ with $\alpha \propto K^2$). The multiscatter contribution increases roughly as α, and, for $K = 10\pi$, can begin to dominate the Born contribution. This is shown in Figures 10 and 11 where we have plotted the Born and multiscatter contributions for $K = 10\pi$ and $K = 4\pi$.

It should be pointed out that the CFSB approximation is also limited to domains where $\alpha L < \pi/2$. Since the average phase variance is given by $<\phi^2> = \alpha L_{eff}$, the point $\alpha L_{eff} = \pi/2$ marks the beginning of the diffusion regime where transport theory must be employed.[2] This boundary will always be crossed for scattering at near grazing angles to the slab, since the effective path length $L_{eff} \rightarrow \infty$ for $\chi_f = 0$ $[\theta_f = \pi/2]$. As K increases, this domain is bounded by $\pm 4°$, $\pm 9°$, $\pm 14°$ and $\pm 20°$ for $K = 4\pi$, 6π, 8π, and 10π respectively for the Kolmogoroff cross sections of Figures 9, 10, and 11.

In Figures 12, 13, and 14 we have plotted the attenuated Born and multiple scattering contributions for the Kolmogoroff spectrum for $\eta = 4$, $K = 8\pi$, and for $L = 0.1$, 1, and 10. For the thin slab case of Figure 12, the multiscatter contribution is less than 1 percent of the total except in the region around the grazing angle at $\chi_f = 0°$. Here the Born term decreases because of the attenuation factor given by Eq. (6) or (7), while the multiscatter term increases due to the increased effective path length. For the medium thick slab of Figure 13, this behavior persists, except that very near $\chi_f = 0°$, attenuation begins to dominate the multiscatter term. For the thick slab case of Figure 14, the multiscatter term is comparable to the attenuated Born term, and the domain where attenuation dominates the multiscatter term near $\chi_f = 0°$ has increased. The angular domains where diffusion scattering is appropriate are given by (-2°, +2°) for the case $L = 1$, and (-15°, +15°) for the case $L = 10$.

The dependence of the total multiple scattering cross section on χ_f is shown in Figure 15 for the case $\eta = 4$, $L = 1$, $K = 2\pi$ for incident angles of $\chi_i = 15°$, 45°, 75°, and 85°. A feature to be observed for the χ_i dependence, as pointed out in I, is that the curves peaked around smaller values of $|\chi_f|$ are broader
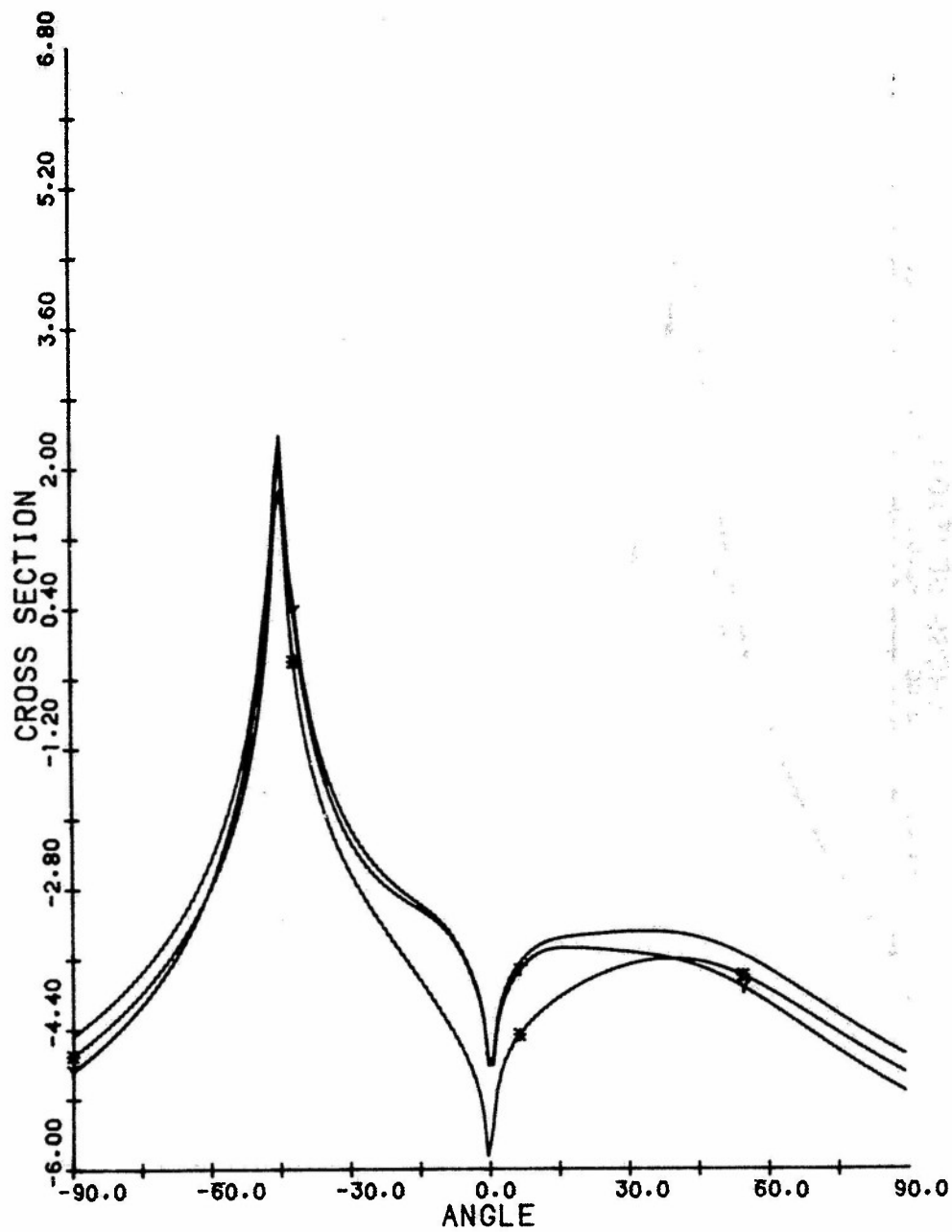
Figure 10. Logarithmic Plot of Born (*), Multiscattering (Y), and Total Cross Sections vs X_f for Kolmogoroff Turbulence for $K = 10\pi$, $\eta = 4$, $L = 10$, $\delta\epsilon = 0.01$

23

Figure 11. Logarithmic Plot of Born (*), Multiscattering (γ), and Total Cross Sections vs χ_f for Kolmogoroff Turbulence for K = 4π, $\eta = 4$, L = 10, $\delta\epsilon = 0.01$

24

Figure 12. Logarithmic Plot of Born (*), Multiscattering (Υ), and Total Cross Sections vs χ_f for Kolmogoroff Turbulence for K = 8π, η = 4, L = 0.1, $\delta\epsilon$ = 0.01
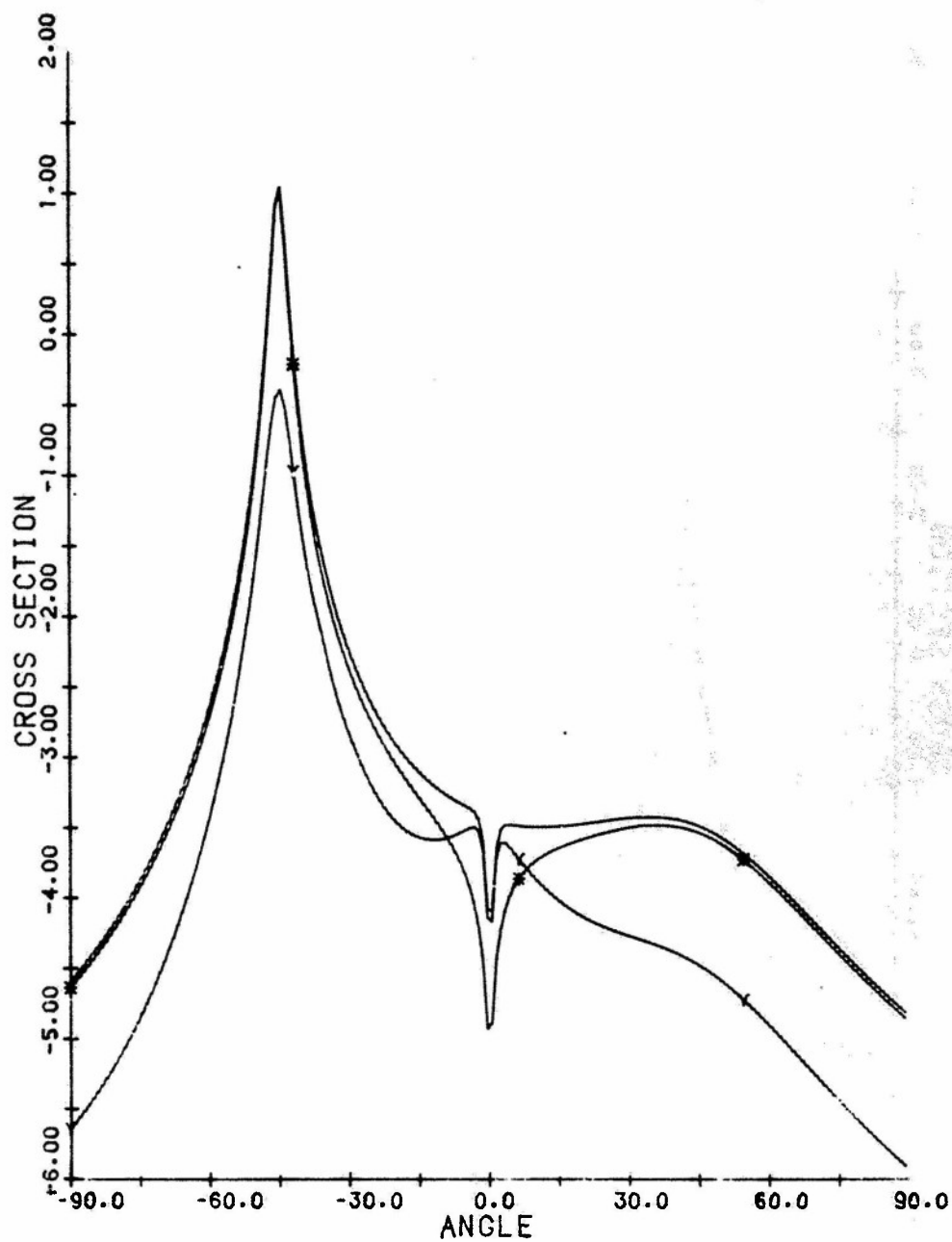
25

Figure 13. Logarithmic Plot of Born (*), Multiscattering (Y), and Total Cross Sections vs X_f for Kolmogoroff Turbulence for $K = 8\pi$, $\eta = 4$, $L = 0.1$, $\delta\epsilon = 0.01$
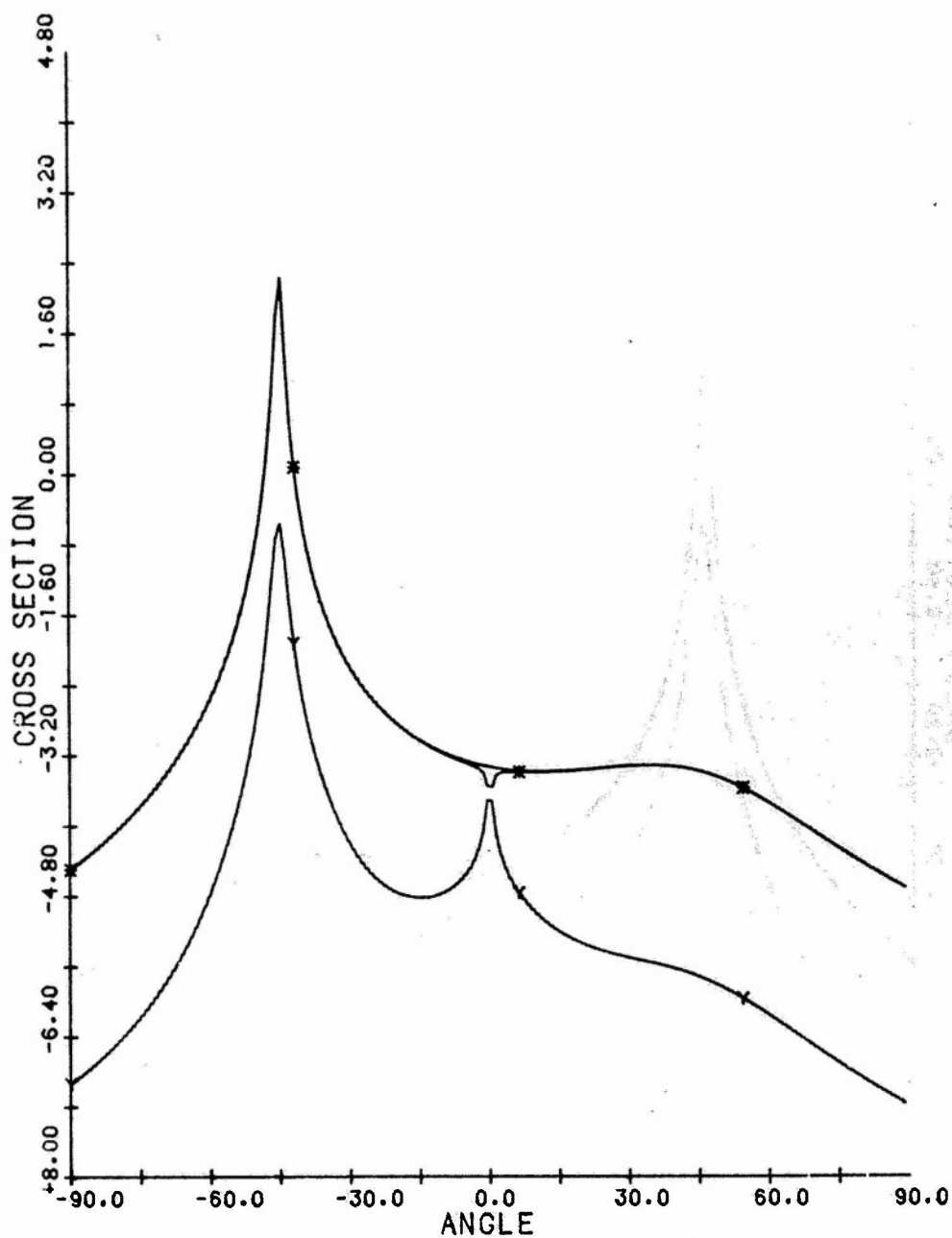
26

Figure 14. Logarithmic Plot of Born (*), Multiscattering (Υ), and Total Cross Sections vs χ_f for Kolmogoroff Turbulence for $K = 8\pi$, $\eta = 4$, $L = 10$, $\delta\epsilon = 0.01$
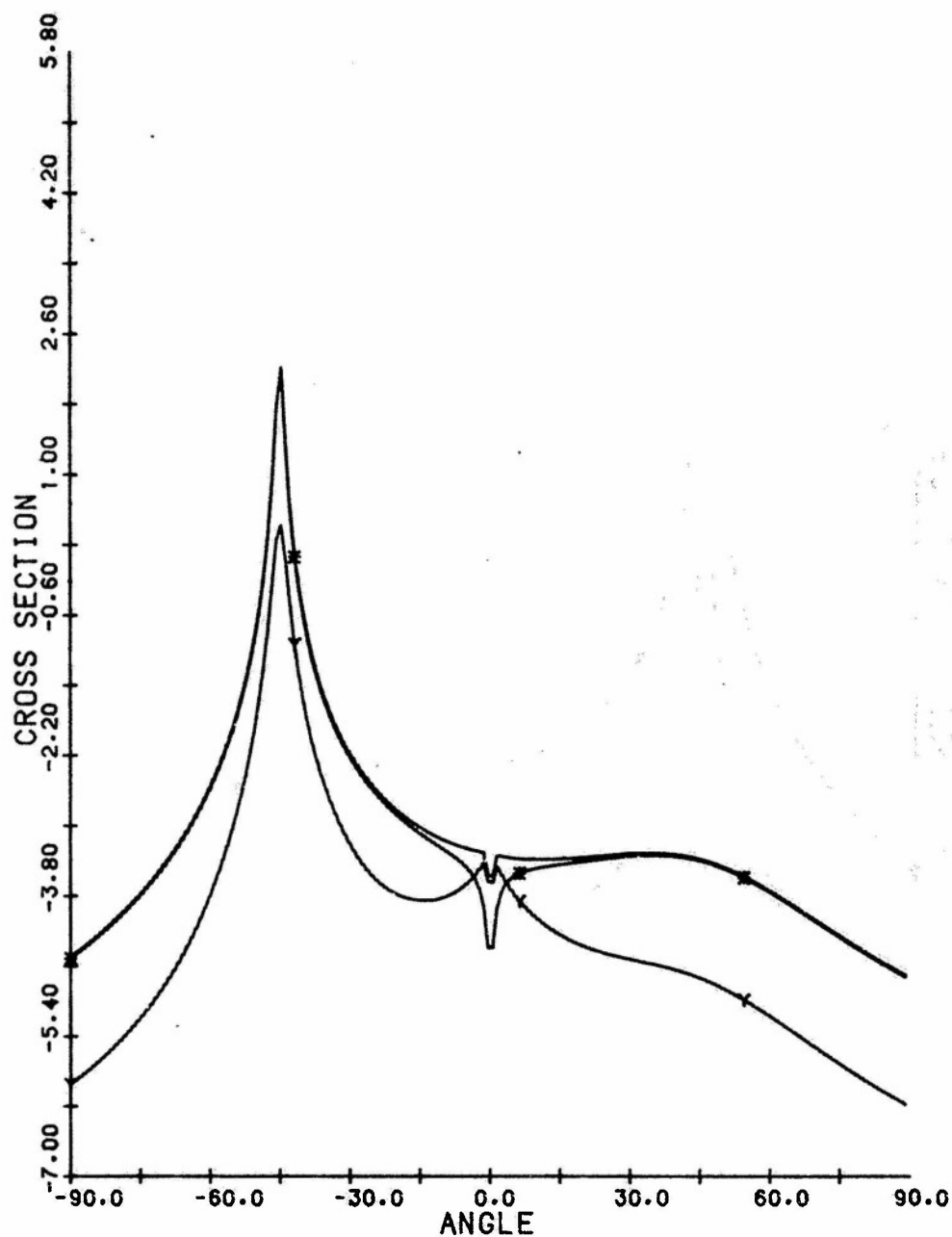
27

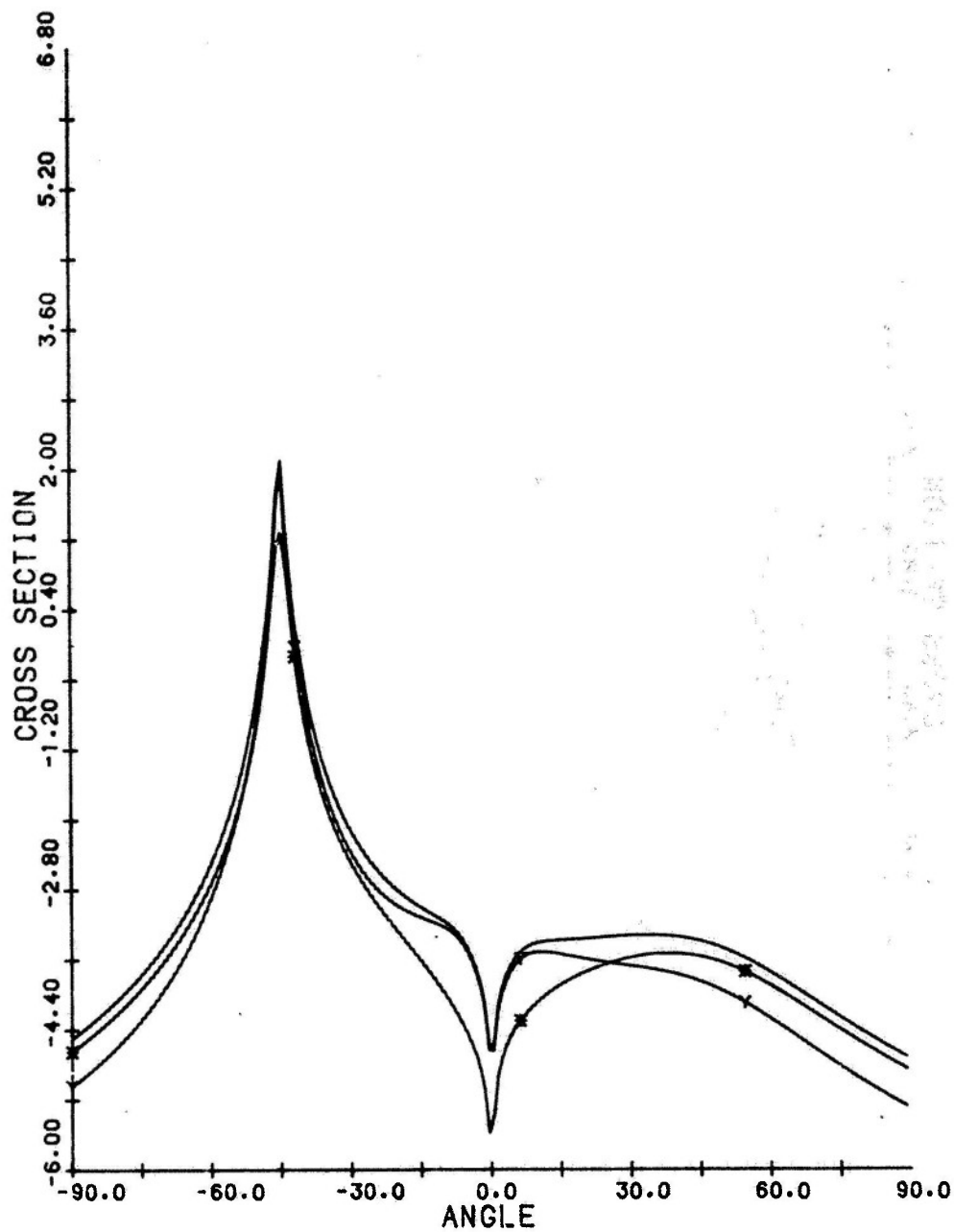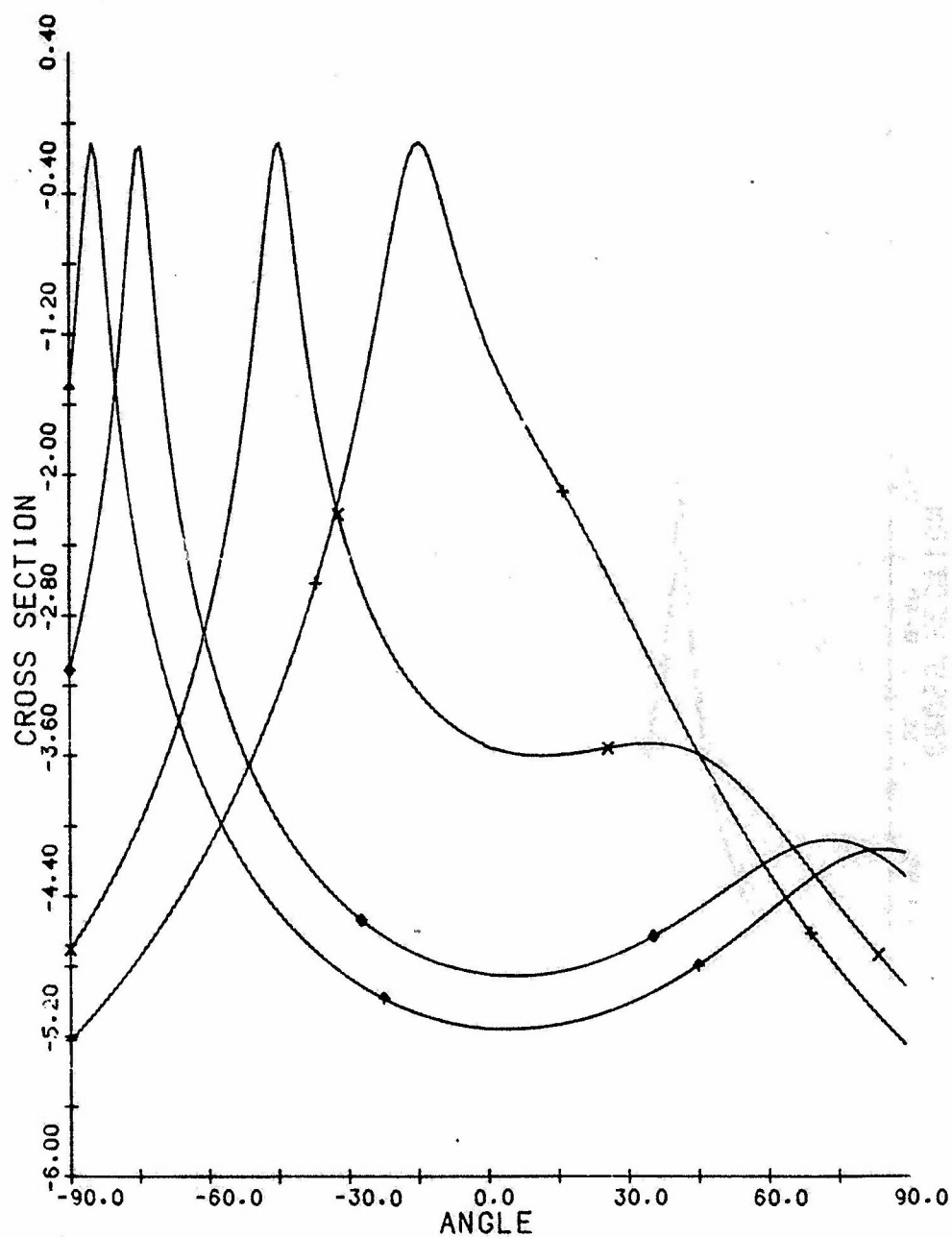Figure 15. Logarithmic Plot of Total Cross Sections vs X_f for Kolmogoroff Turbulence for $X_i = 15°$ (+), $X_i = 45°$ (◊), $X_i = 75°$ (◊), $X_i = 85°$ (✦) With K = 2π, $\eta = 4$, L = 1.0, $\delta\epsilon = 0.01$

since we have plotted with an abscissa proportional to $d\chi_f$ rather than $dK_{f_z} = \sin(\chi_f) \cdot K \cdot d\chi_f$. Thus, increments of χ_f near $\chi_f = 0$ yield smaller changes in dK_{f_z} and therefore broader peaks. The observed decrease in the magnitude of the peak in the specular backscatter direction where $\Delta K_{\parallel} = 0$, is governed by the factor $1/\left[1 + \Delta K_{\perp}^2 \, L_{\perp}^2\right]^{1+\nu} = 1/\left[1 + 4K^2 \sin^2\theta_i \, L_{\perp}^2\right]^{1+\nu}$ which decreases with increasing θ_i.

6. SUMMARY

We have presented a method for calculating multiple scattering cross sections from slabs of arbitrary depth containing a homogeneous distribution of refractive index irregularities. The irregularities are assumed to be aligned along a symmetry axis at a given angle to the slab face and to possess different correlation lengths along and perpendicular to this axis.

Previous calculations that have been carried out for multiple scattering cross sections have been limited to isotropic turbulence having a Gaussian power spectrum and to direct backscattering. The extension to anisotropic Kolmogoroff spectra and scattering at arbitrary angles thus presents a result that corresponds to the general situation encountered in scattering hf waves from ionospheric irregularities.

For correlation functions that depend on a single radial argument $R = \sqrt{\left[(x_1^2 + x_2^2)\, L_{\perp}^2 + x_3^2 \, L_{\parallel}^2\right]}$, projections along a given direction in the medium can be changed by a scale transformation to circularly symmetric form. Numerical evaluation of multiple scattering cross sections for turbulent spectra represented by such correlation functions can then be carried out relatively simply and were evaluated for an anisotropic Kolmogoroff spectrum.

Measurements of ionospheric turbulence spectra[3, 4, 5] tend to indicate a power law spectrum $k^{-\mu}$ with $\mu \simeq 2\text{-}4$. Erukhimov et al[3] further indicate that the factored spectral form of Eq. (28) is supported by their data.

We have noted that the loss of circular symmetry in the plane of the projected correlation function for spectral forms like Eq. (28) requires more extensive numerical calculation because the results of each convolution must be stored as an NxN array rather than as an Nx1 array. If, however, the initial and final scattering angles are such that $\tan\chi_{i,f} \gg 2(L_{\perp}/L_{\parallel})$, the projected correlation function

29

$$\check{D}_\chi(\vec{k}) = \frac{\kappa}{[1 + \vec{k}_\perp^2 L_\perp^2]^{1+\nu}} \cdot e^{-k_1^2 \tan^2(\chi) L_\parallel^2/4}$$

can be approximated by

$$\check{D}_\chi(\vec{k}) \simeq \frac{\kappa}{[1 + k_2^2 L_\perp^2]^{1+\nu}} \cdot e^{-k_1^2 \tan^2(\chi) L_\parallel^2/4}$$

and the two-dimensional convolution integrals factor into two one-dimensional convolution integrals of which the Gaussian part can be evaluated analytically. Using Erukhimov's[2] values of $L_\perp \sim 0.5\,\text{km}$ and $L_\parallel \sim 10.0\,\text{km}$ the above analysis indicates that for $\chi_{i,f} > \sim 20°$ the simpler one-dimensional convolution calculation should be adequate and would constitute an upper bound to the full numerical calculation of multiple scattering contributions.

30

References

1. Yukon, S. P. (1982) Backscatter From Anisotropic Random Media, RADC-TR-82-287, AD-A127873

2. DeWolf, P. A. (1971) Electromagnetic reflection from an extended turbulent medium, Cumulative forward-scatter single-backscatter approximation, IEEE Trans. Antennas Propag. AP 19:254.

3. Erukhimov, L. M., Kosolapenko, V. I., Lerner, A. M., and Myasnikov, E. N. (1982) Form of the inhomogeneity spectrum of the high-latitude ionosphere in the direction of the geomagnetic field, Radio Phys. Quart. Electronics 24:350.

4. Kelley, M. C., Livingston, R. C., Rino, C. L., and Tsunoda, R. T. (1982) The vertical wave number spectrum of topside equatorial spread F: Estimates of backscatter levels and implications for a unified theory, J. Geophys. Res. 87(A7):5217.

5. Ossakow, S. L. (1979) Ionospheric irregularities, Rev. Geophys. Space Phys. 17:521.

31

To show the equivalence of Eqs. (20), (21), and (22), we start from the
expression for the two-dimensional convolution of 2 arbitrary two-dimensional
functions $g(x_1, x_2)$, $f(x_1, x_2)$ whose two-dimensional Fourier transforms
$\widetilde{g}(\vec{p})$, $\widetilde{f}(\vec{p})$ exist.

$$\widetilde{d}(\vec{k}) = \int e^{i\vec{k}\cdot\vec{x}} f(\vec{x}) \, g(\vec{x}) \, d\vec{x} \tag{A1}$$

$$= \int d\vec{x} \int e^{i\vec{k}\cdot\vec{x}} \, e^{-i\vec{q}\cdot\vec{x}} \widetilde{f}(\vec{q}) \int e^{-i\vec{p}\cdot\vec{x}} \widetilde{g}(\vec{p}) \, \frac{d\vec{q}}{(2\pi)^2} \frac{d\vec{p}}{(2\pi)^2} \tag{A2}$$

$$= \frac{1}{(2\pi)^2} \int \delta(\vec{k}-\vec{q}-\vec{p}) \widetilde{f}(\vec{q}) \widetilde{g}(\vec{p}) d\vec{q} \, d\vec{p} \tag{A3}$$

$$= \int \frac{d\vec{q}}{(2\pi)^2} \, \widetilde{f}(\vec{q}) \widetilde{g}(\vec{k}-\vec{q}). \tag{A4}$$

For functions $\widetilde{f}(\vec{p})$ and $\widetilde{g}(\vec{p})$ that depend only on the magnitude of $\vec{p}$, this may be
written as

$$\widetilde{d}(\vec{k}) = \int_0^\infty \frac{q\,dq}{(2\pi)^2} \int_0^{2\pi} d\phi \, \widetilde{f}(q^2) \, \widetilde{g}(k^2 - 2kq\cos(\phi) + q^2). \tag{A5}$$
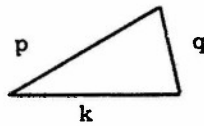
Going back to Eq. (A2), we may re-express this as

33

$$\tilde{d}(\vec{k}) = \int\int_0^\infty \int \rho\, d\rho\; pdpqdq \int\int\int_0^{2\pi} d\phi_q\, d\phi_p\, d\phi$$

$$e^{ik\rho\cos(\phi_k-\phi)}\; e^{-iq\rho\cos(\phi_q-\phi)}\; e^{-ip\rho\cos(\phi_p-\phi)}$$

$$\tilde{f}(q)\,\tilde{g}(p)\,/(2\pi)^4 \tag{A6}$$

$$= \int_0^\infty \rho\, d\rho \int\int_0^\infty \frac{pdpqdq}{(2\pi)^4}(2\pi)^3\, J_0(q\rho)\, J_0(p\rho)\, J_0(k\rho)\, \tilde{f}(q^2)\, \tilde{g}(p^2) \tag{A7}$$

Integrating the Bessel functions over ρ, this may be written as

$$\tilde{d}(\vec{k}) = \frac{\int_0^\infty pdp \int_0^\infty qdq}{(2\pi)^2}\, \tilde{f}(q^2)\, \tilde{g}(p^2)\, \frac{\Delta(p+q-k)}{A} \tag{A8}$$

where $\Delta(p+q-k) = 1$ if p, q, k form the sides of a triangle of area A and

$$\tag{A9}$$

zero otherwise. Expressing the area of the triangle as $A = s(s-k)(s-p)(s-q)$ where $s = \dfrac{k+p+q}{2}$, this may be re-expressed as

$$\tilde{d}(k) = \frac{\int_0^\infty pdp \int_0^\infty qdq}{(2\pi)^2}\, \frac{\tilde{f}(q^2)\, \tilde{g}(p^2)\, \Delta(p+q-k)}{[s(s-k)(s-p)(s-q)]} \tag{A10}$$

$$= \int_0^\infty \frac{pdp}{(2\pi)^2} \int_{|p-k|}^{|p+k|} qdq\, \frac{4\tilde{f}(p^2)\, \tilde{g}(q^2)}{[(p+k)^2-q^2]^{1/2}[q^2-(p-k)^2]^{1/2}} \tag{A11}$$

To show the equivalence of this expression with Eq. (A5) in another way, we let $z=q^2$, $a = (p-k)^2$, $b = (p+k)^2$, and re-express Eq. (A11) as

34

$$\widetilde{d}(\vec{k}) = \frac{1}{(2\pi)^2} \int_0^\infty p\,dp \quad \widetilde{f}(p^2) \quad 2\int_{z=a}^{z=b} \frac{dz\, \widetilde{g}(z)}{\sqrt{(b-z)(z-a)}} \tag{A12}$$

Changing variables to $z = \frac{b+z}{2} + \frac{(b-a)}{2} x$ yields

$$\widetilde{d}(\vec{k}) = \frac{1}{(2\pi)^2} \int_0^\infty p\,dp\, \widetilde{f}(p^2) \int_{x=-1}^{x=1} \frac{dx}{\sqrt{1-x^2}}\, \widetilde{g}(p^2 + k^2 + 2pkx). \tag{A13}$$

Letting $x = \cos\phi$ then gives

$$\widetilde{d}(\vec{k}) = \frac{1}{(2\pi)^2} \int_0^\infty p\,dp\, \widetilde{f}(p^2) \int_0^{2\pi} d\phi\, \widetilde{g}(p^2 + k^2 - 2pk\cos\phi)$$

$$= \frac{1}{(2\pi)^2} \int_{-\infty}^\infty d\vec{p}_\perp\, \widetilde{f}(\vec{p}^2)\, \widetilde{g}((\vec{p} - \vec{k})^2) \tag{A14}$$

which is Eq.(A5).

35

MISSION
of
Rome Air Development Center

RADC plans and executes research, development, test
and selected acquisition programs in support of
Command, Control, Communications and Intelligence
(C^3I) activities. Technical and engineering
support within areas of competence is provided to
ESD Program Offices (POs) and other ESD elements
to perform effective acquisition of C^3I systems.
The areas of technical competence include
communications, command and control, battle
management, information processing, surveillance
sensors, intelligence data collection and handling,
solid state sciences, electromagnetics, and
propagation, and electronic, maintainability,
and compatibility.